

## Article

# Geodynamic Settings of Late Paleozoic–Early Mesozoic Granitoid Magmatism at the Arctic Continental Margins: Insights from New Geochronological and Geochemical Data from the Taimyr Peninsula

Mikhail Yu. Kurapov <sup>1,2</sup>, Dmitry L. Konopelko <sup>1,\*</sup> , Yuriy S. Biske <sup>1</sup>, Vasily F. Proskurnin <sup>2</sup>, Sergei V. Petrov <sup>1</sup>, Maria A. Proskurnina <sup>2</sup>, Yevgeny Yi. Berzon <sup>2</sup>, Victoria B. Ershova <sup>1,3</sup> , Stepan V. Berzin <sup>1</sup>  and Sergey Yu. Stepanov <sup>2</sup>

<sup>1</sup> Institute of Earth Sciences, Saint Petersburg State University, Universitetskaya nab. 7/9, St. Petersburg 199034, Russia; m.kurapov@spbu.ru (M.Y.K.); gbiskeh@yandex.ru (Y.S.B.); petrov64@gmail.com (S.V.P.); v.ershova@spbu.ru (V.B.E.); sbersin@yandex.ru (S.V.B.)

<sup>2</sup> A.P. Karpinsky Russian Geological Research Institute (VSEGEI), Sredniy Prospect 74, St. Petersburg 199106, Russia; vasily\_proskurnin@vsegei.ru (V.F.P.); maria\_proskurnina@vsegei.ru (M.A.P.); evgeniy\_berzon@vsegei.ru (Y.Y.B.); stepanov-1@yandex.ru (S.Y.S.)

<sup>3</sup> Geological Institute, Russian Academy of Sciences, Pyzhevsky Lane 7, Moscow 109017, Russia

\* Correspondence: konopelko@inbox.ru or d.konopelko@spbu.ru



check for updates

**Citation:** Kurapov, M.Y.; Konopelko, D.L.; Biske, Y.S.; Proskurnin, V.F.; Petrov, S.V.; Proskurnina, M.A.; Berzon, Y.Y.; Ershova, V.B.; Berzin, S.V.; Stepanov, S.Y. Geodynamic Settings of Late Paleozoic–Early Mesozoic Granitoid Magmatism at the Arctic Continental Margins: Insights from New Geochronological and Geochemical Data from the Taimyr Peninsula. *Minerals* **2024**, *14*, 423. <https://doi.org/10.3390/min14040423>

Academic Editors: Michel Villeneuve, Chengjun Zhang, Jiaolong Zhao and Pengju He

Received: 18 February 2024

Revised: 11 April 2024

Accepted: 17 April 2024

Published: 19 April 2024



**Copyright:** © 2024 by the authors. Licensee MDPI, Basel, Switzerland. This article is an open access article distributed under the terms and conditions of the Creative Commons Attribution (CC BY) license (<https://creativecommons.org/licenses/by/4.0/>).

**Abstract:** Despite significant progress in Arctic geological studies, a number of principal questions concerning the Paleozoic collisional events remain unanswered. Therefore, the Taimyr Peninsula, representing the only outcropped high Arctic region where magmatic complexes, formed by Hercynian collision between the Siberian Craton and the Kara Block, are well exposed, is crucially important. In this paper we report new geochemical and geochronological data for intrusions in the poorly studied northeastern part of the Taimyr Peninsula. The obtained results in combination with published data show that supra-subduction magmatism at the southern active margin of the Kara Block continued from ca. 345 to 285 Ma (Early Carboniferous to Early Permian), and was followed by a post-collisional magmatic pulse that affected the whole Taimyr across terrane boundaries at ca. 280 Ma in the Early Permian. After cessation of the post-collisional magmatism at ca. 265 Ma, the Taimyr experienced extension, and voluminous magmatic series associated with a Siberian mantle plume were formed between 251 and 228 Ma during the Triassic. The studied post-collisional and plume-related intrusions of the Northeastern Taimyr are generally classified as evolved high-K I-type granites with adakitic affinity. The latter is a regional feature because the majority of the analyzed plume-related granitoids are geochemically similar to high potassium continental adakites. It is suggested that the adakitic geochemical characteristics of the plume-related granitoids resulted from melting of hydrated mafic lower crustal protoliths and were controlled by the source lithology. Comparison of the new results with data available for adjacent areas allows for correlation of terranes on a regional scale and sheds light on the evolution of the Arctic continental margins in general. In the Early–Middle Paleozoic, the Kara Block was part of a continental terrane that formed at the northern edge of Baltica as a result of Neoproterozoic Timanian orogeny. In the Early Carboniferous, the southern margin of Kara turned into an active margin, while its inferred continuation in the eastern Uralian margin of Baltica remained a passive margin until the Early Permian. This discrepancy can be explained by dextral displacement of Kara relative to Baltica that took place in the Early Carboniferous and was later accommodated by the formation of the Taimyr collisional belt in the course of the Early Permian collision between Kara and Siberia. After collision, the Taimyr was incorporated into the northern Eurasian margin as an uplifted block that experienced surface erosion and supplied clastic material in surrounding basins.

**Keywords:** Arctic continental margins; Kara block; Taimyr peninsula; late Paleozoic collision; Siberian LIP; granite; adakite; U–Pb age

### 1. Introduction

The Arctic Ocean includes a vast area of Cenozoic oceanic lithosphere and several deep-sea troughs filled with Jurassic–Cenozoic sediments [1–4]. The ocean is surrounded by extensive shelf zones, where pre-Mesozoic continental basement is hidden under thick Meso-Cenozoic sedimentary cover and remains insufficiently studied. The basement of the Arctic margins consists of continental terranes of various size and origin including Archean and Paleoproterozoic cratons, Neoproterozoic microcontinents derived from Rodinia, and Paleozoic orogenic belts [5–7] (Figure 1). Phanerozoic magmatic rocks, which provide one of the most important proxies to decipher the tectonic evolution, make up significant portions of the Arctic crust, and formed in the course of the Caledonian [8–13], Ellesmerian [14], and Hercynian [15–19] orogenic cycles during the Paleozoic, and as a result of the formation of Siberian Traps [20–25] and High Arctic (HALIP) [26–30] Large Igneous Provinces during the Mesozoic (Table 1).

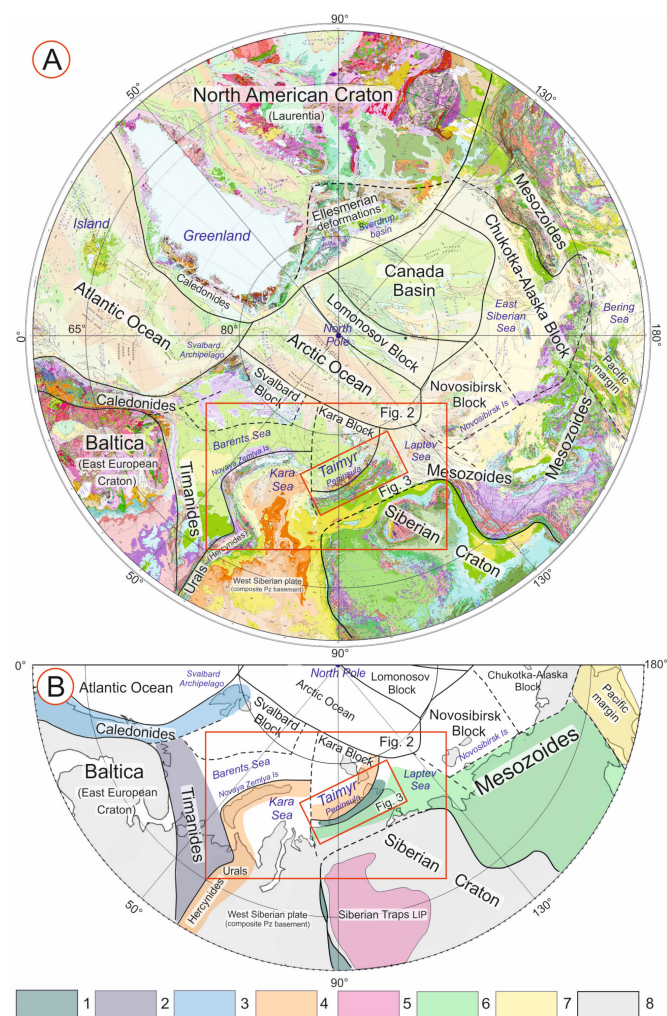


**Figure 1.** Geology and tectonics of the Arctic continental margins. (A) Circumpolar geological map of the Arctic [31] showing major tectonic units and location of study area in the Taimyr Peninsula. (B) Schematic tectonic map of the Western Hemisphere demonstrating major orogenic belts formed in the Neoproterozoic and Phanerozoic. Legend: 1—Baikalides at Siberian margins; 2—Timanides; 3—Caledonides of Norway and Svalbard; 4—Hercynian fold belts and sutured continental margins of Urals and Kara, and Early Mesozoic fold belt of Novaya Zemlya; 5—generalized surficial distribution of flood basalts and associated rock-types of Siberian Traps LIP within Siberian Craton after [32]; 6—Mesozoides (Cimmerides) of NE Russia and deformed Mesozoic sediments of the Southern Taimyr Domain; 7—Alpine accretionary orogenic belts at Pacific margins; 8—cratons, microcontinental blocks and young plates with relatively underformed sedimentary cover.

**Table 1.** Major stages of tectono-magmatic evolution of the Arctic continental margins.

Orogenic Cycle	Collisional Event/LIP	Timing of Collision/LIP	Typical Magmatic Series at Arctic Continental Margins
	Opening of the Arctic Ocean with currently active spreading center in Paleocene		
Cimmerian (Mesozoides)	High Arctic Large Igneous Province (HALIP)	Cretaceous	Flood basalts and doleritic sills in continental shelf zones of the Arctic Ocean.
	Formation of giant Mesozoic orogenic collage between Siberia and North American Craton (Laurentia).	Late Jurassic–Early Cretaceous	Granitoid magmatism in Chukotka-Alaska Block and in Mesozoic orogenic collage of NE Russia.
	Siberian Traps Large Igneous Province (LIP)	Permo–Triassic boundary	Predominantly granitoid magmatism at the periphery of Siberian plume in Northern and Central Taimyr. Flood basalts and doleritic sills of Siberian Traps LIP in the central part of the plume within Siberian Craton.
Hercynian	Collision of Baltica with Paleo-Kazakhstan and Siberia, collision of Kara Block with Siberia and collision of Laurussia with Gondwana to form the supercontinent of Pangaea.	Late Carboniferous–Early Permian	Supra-subduction and post-collisional granitoid magmatism in Northern and Central Taimyr domains. Hercynian granitoids of Polar Urals.
Ellesmerian	Accretion of micro-continental blocks to the margin of North American Craton (Laurentia).	Late Devonian–Early Carboniferous	Granitoid magmatism in Chukotka-Alaska Block.
Caledonian	Collision of Baltica with North American Craton (Laurentia).	Late Ordovician–Silurian	Granitoid magmatism in Caledonides of Norway and Svalbard Archipelago.
Timanian	Collision of Svalbard Block with Baltica.	Neoproterozoic–Early Paleozoic (Ediacaran to Early Cambrian)	Granitoid intrusions of Polar Urals, Novaya Zemlya Isl., and in the Timanides comprising the basement of Pechora basin.
Baikalian	Collision of Kara Block with Siberia and other collisional events at Siberian margins.	Neoproterozoic (Ediacaran)	Ediacaran granitoids of Central Taimyr Domain and other fold belts along Siberian margins.

Despite significant progress in the investigations into tectonic evolution of the Arctic during recent decades [1,33,34], a number of principal questions concerning the Paleozoic collisional events remain unanswered. Therefore, the Taimyr Peninsula, representing the only outcropped area where the structures, formed by Hercynian collision between the Siberian Craton and the Kara Block, are well exposed and accessible for study, is crucially important (Figures 1–3). Paleozoic granitoid magmatism of the Taimyr Peninsula has been addressed in a number of studies [9,15,16,18,20–22,35–42], and several recent works emphasized the importance of the Early Mesozoic intrusive series [9,15,16,20,22,35,39].

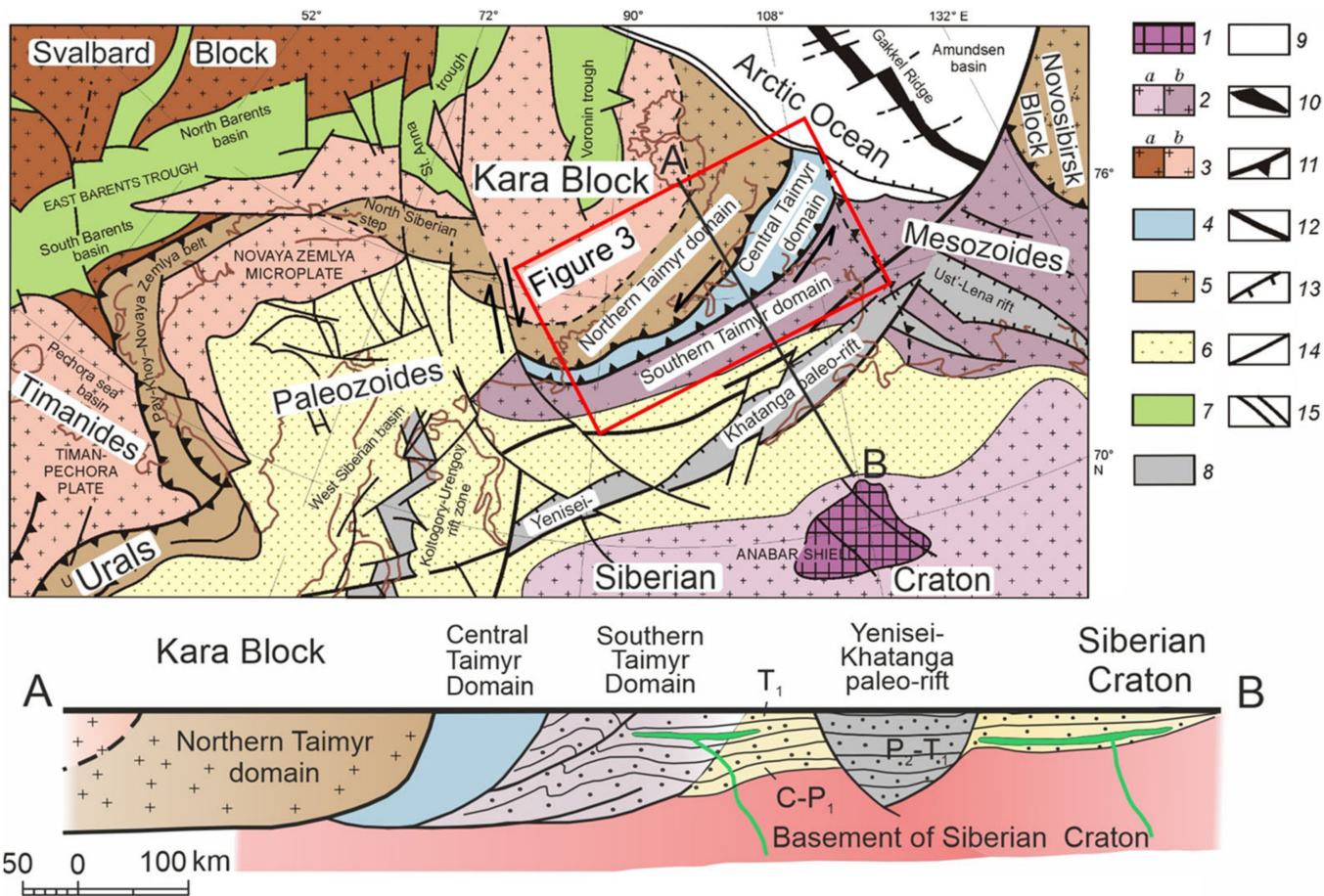
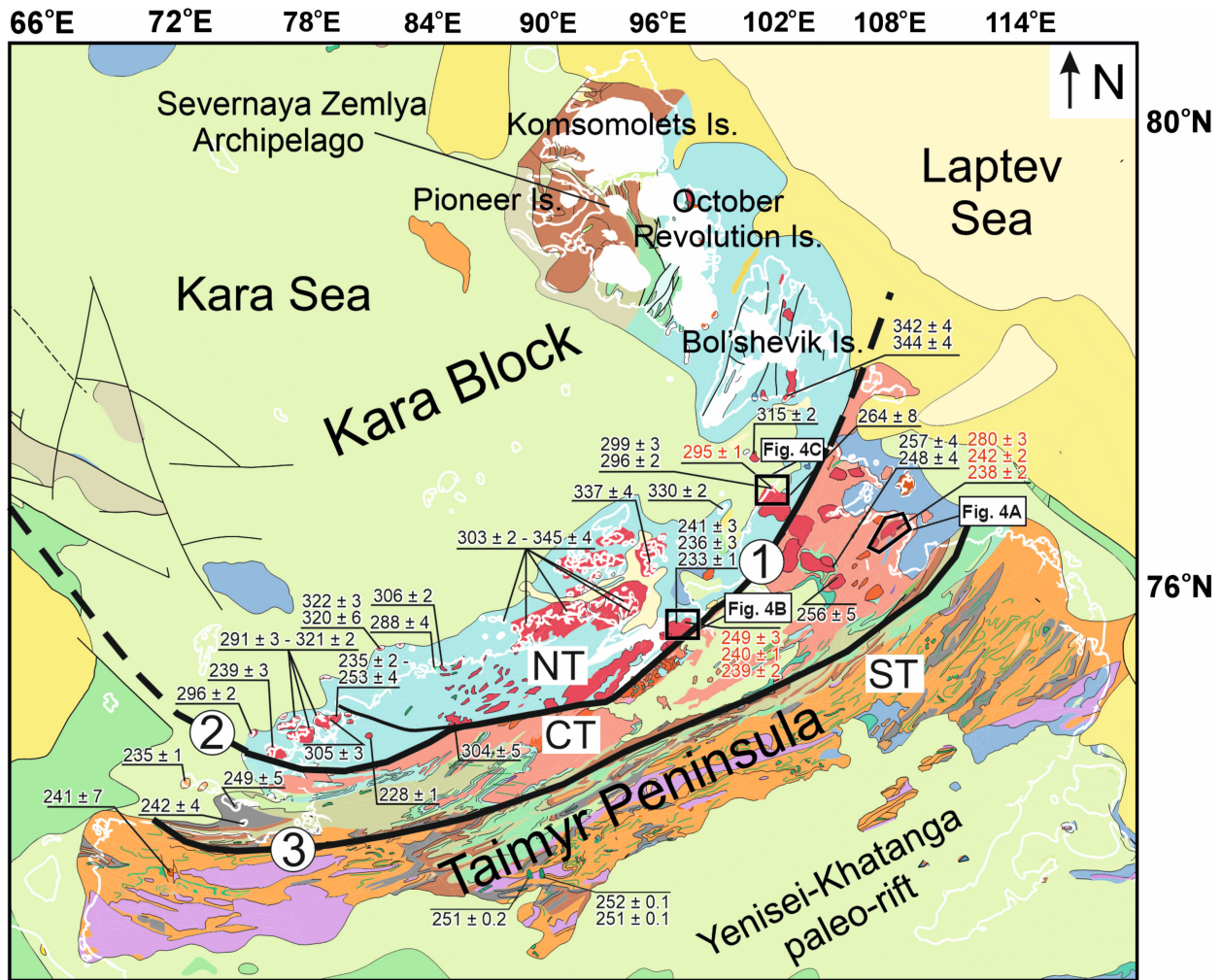


**Figure 2.** Simplified tectonic map of the Svalbard–Kara region and adjacent areas in the Arctic with schematic cross section through the Taimur Peninsula. After [7], modified by the authors. Legend: 1—Precambrian metamorphic rocks of the Anabar Shield; 2—sedimentary cover of the Siberian Craton: (A) undeformed and (B) subjected to Mesozoic deformations; 3—microcontinents with (A) Meso-Neoproterozoic and (B) Neoproterozoic–Early Paleozoic (Timanian) basement; 4—Neoproterozoic (Baikalian) accretionary orogen of Central Taimyr Domain; 5—Hercynian fold belt and sutured continental margins of Urals and Kara, and Early Mesozoic fold belt of Pay-Khoy–Novaya Zemlya; 6—Meso-Cenozoic sedimentary cover of the West Siberian plate with Paleozoic basement and northern part of the Siberian Craton; 7—deep-sea troughs; 8—Triassic intra-continental paleo-rifts; 9—Cenozoic oceanic crust of the Arctic Ocean; 10—Mid-ocean Ridge; 11—major thrusts; 12—strike-slip and transform faults; 13—normal faults; 14—other undivided faults; 15—edge of continental slope.



**Legend**

Neogene	Triassic	Silurian	Triassic mafic intrusion
Paleogene	Permian	Ordovician	Late Paleozoic - Early Mesozoic felsic intrusion
Upper Cretaceous	Carboniferous	Cambrian	Neoproterozoic felsic intrusion
Lower Cretaceous	Devonian	Paleozoic undivided	Faults
Jurassic			Assumed faults

- ① Main Taimyr fault      NT - Northern Taimyr domain
- ② Diabasic fault        CT - Central Taimyr domain
- ③ Pyasina-Faddey fault   ST - Southern Taimyr domain

**Figure 3.** Simplified geological map of the Taimyr Peninsula and Severnaya Zemlya Archipelago showing locations of studied areas and ages of intrusions (modified after [43–45]). Ages obtained in this study are shown in red. Other ages from [9,15,16,18,20–22,35,38–41,46].

Herein, we present new geochemical data and results of sensitive high-resolution ion microprobe (SHRIMP) U–Pb zircon dating obtained for three Late Paleozoic–Early Mesozoic intrusions located in the poorly studied northeastern part of the Taimyr Peninsula (Figure 3). The new data constrain the age and characterize the geochemistry of supra-subduction, post-collisional and plume-related granitoid series associated with the evolution of the Taimyr–Severnaya Zemlya fold-and-thrust belt during the Late Paleozoic–Early Mesozoic times. Particular emphasis is made on the geochemical affinity of Taimyr granitoids to

high potassium adakites typical of the areas with thickened continental crust, such as Tibet [47–52]. Comparison of the new results with data available for adjacent areas of the Taimyr Peninsula allows for correlation of terranes on a regional scale and sheds light on the Paleozoic and Mesozoic evolution of the Arctic continental margins in general.

## 2. Geological Setting of the Arctic Continental Margins

Major Precambrian continental blocks comprising the Arctic continental margins in the Eastern Hemisphere include, from west to east, the Svalbard block, the Kara block, which is partially exposed in the Taimyr Peninsula and Severnaya Zemlya Archipelago, as well as the Novosibirsk and Chukotka-Alaska blocks located to the east [1,5,53] (Figure 1). These terranes were separated in the Neoproterozoic from the Rodinia supercontinent [54] as either a single continent, Arctida [55,56], or as individual microcontinents [57,58].

It is generally accepted that accretion of the Svalbard block to Baltica took place in the latest Neoproterozoic–Early Cambrian and formed the orogenic belt of Timanides comprising part of the basement of the northeastern Europe and the Barents Sea shelf, in particular. Collisional events of similar or slightly older (Baikalian) age also occurred at Siberian margins where they formed the Central Taimyr Domain and other Neoproterozoic belts along the western margin of Siberia (e.g., [56,58]) (Figure 2). Based on detrital zircon studies, it has been established that during the latest Neoproterozoic (630–550 Ma) an active continental margin also developed in the Kara Block. However, recent tectonic reconstructions suggest that in the Neoproterozoic, the Kara Block was separated from the Siberian Craton and represented either a part of Arctida or an isolated microcontinent [59,60].

The closure of the Japetus Ocean in the late Ordovician–Early Silurian was manifested as a Caledonian collisional event along the Barents Sea margin in the western Svalbard Block. In the easternmost parts of the Arctic, the closure of the Japetus Ocean probably took place in the Late Silurian and Devonian, and formed a collisional structure known as the Ellesmerian orogenic belt along the Chukotka-Alaska block and Canadian Arctic [58,61].

The Carboniferous–Permian Hercynian collisional orogeny resulted in the closure of the Paleo-Asian Ocean separating Siberia and Baltica (Laurussia) and final incorporation of Siberia into the Pangaea supercontinent. Hercynian collision created the Uralian orogenic belt at the Baltica margin and also affected various Arctic terranes. However, in contrast to the Urals, Hercynian structures at Arctic margins are mostly unexposed making the Taimyr Peninsula a unique place where the collisional belt separating the Kara Block and Siberia is accessible for study (Figure 2).

After Hercynian collision, at the Permo–Triassic boundary, the Taimyr experienced another major episode of magmatism triggered by formation of the Siberian Traps Large Igneous Province in the northwestern part of the Siberian Craton [20–25] (Figure 1B). This event formed numerous mafic sills in the Southern Taimyr and a number of granitoid intrusions in the Central and Northern Taimyr Domains (Figure 3).

## 3. Geology of the Taimyr Peninsula

The Taimyr Peninsula and, located to the north, the Severnaya Zemlya Archipelago lie on the northern edge of Siberia, between the Laptev and Kara seas. This large piece of land, where pre-Mesozoic basement rocks are exposed, stretches from east to west for more than a thousand kilometers. The Yenisei–Khatanga paleo-rift separates the Taimyr Peninsula from the Siberian Craton located to the south (Figure 3).

The Taimyr–Severnaya Zemlya fold-and-thrust belt is subdivided into three major tectonic units or domains, namely the Southern, Central and Northern Domains (Figure 3). The Northern Domain is separated from the Central Domain by the Main Taimyr and Diabasic regional faults, and the Central Domain is separated from the Southern Domain by the Pyasina–Faddey fault. All three major faults represent regional-scale thrusts dipping to the northeast (Figure 3) [18,62].

The Northern Taimyr Domain is mainly composed of Early Paleozoic (mostly Cambrian and Ordovician) sedimentary rocks metamorphosed under greenschist- to amphibolite-

facies conditions [18,43]. These metasediments were originally mapped as Proterozoic in age [17,19,63], however, recent detrital zircon studies have shown that the depositional ages of these rocks are predominantly Cambrian [59,64–66]. The Northern Taimyr Domain and Severnaya Zemlya Archipelago are interpreted as parts of the Kara microcontinent where the Early Paleozoic sediments were deposited in a passive margin geodynamic setting. Early Paleozoic sedimentary rocks of the Northern Taimyr Domain are intruded by voluminous Carboniferous to Triassic granitic plutons occupying up to 20% of the Northern Domain territory at the present-day erosion surface [9,15,16,22,35,36,38,39,41].

The Central Taimyr Domain was initially interpreted as a collage of diverse terranes accreted to the continental margin of Siberia during the Neoproterozoic [62,67,68]. An alternative point of view suggests that the Central Domain was already formed by accretion to the Siberian margin in the Mesoproterozoic, and during the Neoproterozoic developed as an active continental margin [69]. In the latest Neoproterozoic it was transformed into a passive margin where the deposition of the shelf sediments continued until the Late Paleozoic. The Central Domain consists of Meso- and Neoproterozoic sediments, ophiolite fragments, and magmatic rocks metamorphosed under greenschist- to amphibolite-facies conditions, and overlain by Ediacaran to Silurian sedimentary succession [18,40,43,70]. Importantly, the Central Taimyr Domain is intruded by Permian–Early Triassic granites and Early Triassic dolerite dykes and sills, correlated with synchronous magmatism of the Siberian Traps Large Igneous Province (LIP) [18,21,22,35,40]. Jurassic–Lower Cretaceous sediments have discontinuous distribution and fill local depressions in both the Northern and Central Taimyr domains [43].

The Southern Taimyr Domain represents part of the Paleozoic passive margin of the Siberian Craton. The Ordovician to Triassic sedimentary sequence, which is exposed within the Southern Domain, was intruded by latest Permian–Early Triassic dykes and sills associated with Siberian Traps LIP. These intrusions were variably deformed during subsequent Mesozoic events [18,20].

The Taimyr–Severnaya Zemlya fold-and-thrust belt formed as a result of collision between the Kara Block and Siberia in the Late Carboniferous–Early Permian [15,16,35,46,62]. Compression and tectonic activity terminated in the Early Permian when the Kara Block, including the Taimyr–Severnaya Zemlya areas, was accreted to the northern margin of the Siberian Craton [15,35]. Termination of compression was followed by an extensional regime that affected the Siberian margins and the West Siberian basin in the Late Permian–Early Triassic [71–75]. In Taimyr, this extension was manifested by the opening of the Yenisei–Khatanga paleo-rift (Figure 3), and other indications of extensional tectonics described elsewhere in Taimyr [75].

#### 4. Description of the Studied Intrusions

Extreme climatic conditions and the remote location of the Taimyr Peninsula make data acquisition in this area a challenging task. Therefore, every newly investigated intrusion provides unique new information on this region. Herein, we present first data from three intrusions, located in the Central (Peka River intrusion) and Northern Taimyr domains (Olenya and Tessema River intrusions), collected in the course of geological mapping projects between 2008 and 2021.

The Peka River intrusion is located in the Central Taimyr domain (Figures 3 and 4A). It is a relatively small granitoid body occupying an area of ca. 70 km<sup>2</sup>. The intrusion is composed of granitoid rocks intruded in three phases: the first phase comprises porphyritic granites and granosyenites, the second—porphyritic granite, the third—differently oriented dikes and veins of aplite, pegmatoid granite, and less commonly pegmatite. The contacts with the host rocks are steep and sinuous. Large rhyolitic xenolith (at least 200 m across) is exposed in the southwestern part of the intrusion (Figure 4A).

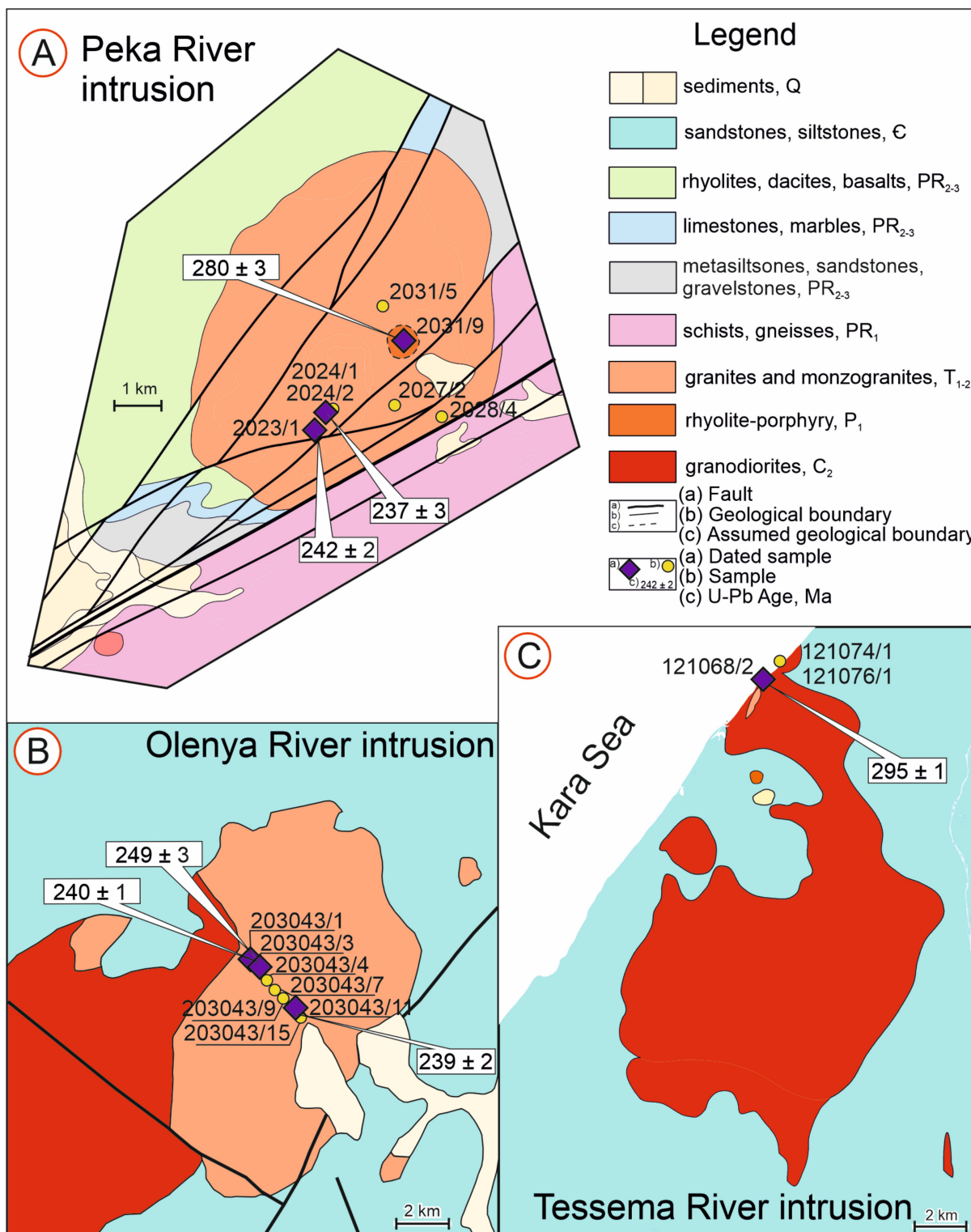


**Figure 4.** Simplified geological maps of the studied intrusions showing location of sampling points and obtained ages: (A) Peka River intrusion; (B) Olenya River intrusion; (C) Tessema River intrusion. Compiled by the authors.

The Olenya River intrusion is located in the Northern Taimyr Domain (Figures 3 and 4B). It has an area of about 125 km<sup>2</sup>. The intrusion is oval in shape; the contacts are plain, sharp, and sub-vertical. The first intrusive phase, comprising the main volume of the intrusion, is represented by porphyritic biotite granite. Granites of the second phase

make up small stocks and dikes. In composition they correspond to medium-grained biotite granite-porphyry, granite, and leucogranite. Aplitic varieties are developed in the endocontact. Rocks of the third phase are represented by pegmatite, aplite, and fine- to medium-grained granite porphyries. At the final stage, the muscovite-quartz-feldspar veins and hydrothermal-metasomatic veinlets of fluorite-pyrite-muscovite-quartz composition were formed. Granitoids of the third phase host molybdenite and chalcopyrite-pyrite mineralization associated with metasomatic veins.

The Tessema River intrusion is located in the Northern Taimyr Domain on the shore of the Kara Sea (Figures 3, 4C and 5). It has an area of about 650 km<sup>2</sup>, irregular shape, and sharp sub-vertical contacts. The rocks of the Tessema River intrusion have a relatively heterogeneous composition varying from tonalite to leucogranite. The pluton intrudes Cambrian metasedimentary rocks and is overlain by Late Jurassic–Early Cretaceous sediments of the Mukha Formation, Paleogene sediments, and Quaternary loose sediments. The granites are intruded by the Early Triassic dolerite dikes.



**Figure 5.** Photographs illustrating exposure and structure of granites of the Tessema River intrusion: (A) general view of sharp-angled granite boulders on the shore of the Kara Sea; (B) close up view of granite fragments; (C,D) photomicrographs of granite in cross-polarized light.

## 5. Analytical Procedures

U-Pb zircon dating was carried out at the Center of Isotopic Research of the Russian Geological Research Institute (VSEGEI) in St. Petersburg. Separation of zircon grains was performed according to the standard procedure including crushing of rock fragments to approximately 0.25 mm in size, a centrifugal concentration, removing of the highly magnetic minerals, and processing with heavy liquids. The handpicked zircon grains were mounted in the epoxy resin discs along with fragments of the TEMORA and 91,500 zircon standards. The discs were polished to expose centers of zircon grains. Cathodoluminescent (CL) images were used to guide the selection of analysis points. U-Th-Pb isotope analyses of zircon grains were made using a Sensitive High-Resolution Ion Microprobe (SHRIMP-II) by Australian Scientific Instruments, Canberra, Australia. Each analysis consisted of four scans through the mass range. The diameter of the spot was about 30  $\mu\text{m}$ , and the primary beam current was about 4 nA. The data were reduced in a manner similar to that described by Williams (1998) [76], utilizing the SQUID Excel Macro of Ludwig (2000) [77]. The Pb/U ratios have been normalized relative to a value of 0.0668 for the  $^{206}\text{Pb}/^{238}\text{U}$  ratio of the TEMORA 1 standard. The zircon standard 91,500, with a U concentration of 81.2 ppm and an accepted  $^{206}\text{Pb}/^{238}\text{U}$  age of 1065 Ma, was used as a “U-concentration” standard [78]. Uncertainties of individual analyses (ratios and ages) were calculated at a level of  $\pm 2\sigma$ . The ISOPLOT program was used to construct concordia diagrams [79].

Whole-rock samples were analyzed for major and trace elements at the Central Laboratory of VSEGEI. All samples underwent conventional crushing and grinding. The major oxide concentrations were determined on an ARL 9800 XRF spectrometer by Thermo Fisher Scientific, Waltham, MA USA. The contents of trace elements (including REE) were determined on an OPTIMA 4300DV by PerkinElmer, Waltham, MA USA emission spectrometer and an ELAN 6100 DRC mass spectrometer by PerkinElmer, Waltham, MA USA. Analytical uncertainties for major and trace elements were generally better than 5%. Reproducibility and accuracy of the OMAC sample suite are well within 10%. Petrographic study of rocks was performed using Olympus BX51 by Olympus Shinjuku, Japan and Leica DM4000 P LED by Leica microsystems, Wetzlar, Germany optical microscopes.

## 6. Petrography and Geochemistry

We present a petrographic description and first major and trace element data for 18 magmatic rocks from three intrusions located in the Northeastern Taimyr area. Coordinates of sampling points and analytical results are given in Supplementary Table S1 and shown in schematic geological maps of intrusions in Figure 4. Photographs illustrating exposure and structure of the studied granites are presented in Figure 5 and in Supplementary Figure S1. Major and trace element data are plotted in classification and discrimination diagrams (Figures 6–9) where the analyzed rocks are subdivided into three groups: subduction-related (Tessema River intrusion), post-collisional (xenolith from Peka River intrusion), and plume-related granites (Olenya and Peka River intrusions). Published data from granitoid intrusions of adjacent Taimyr regions are included in the dataset and shown in Figures 6–9 for comparison.

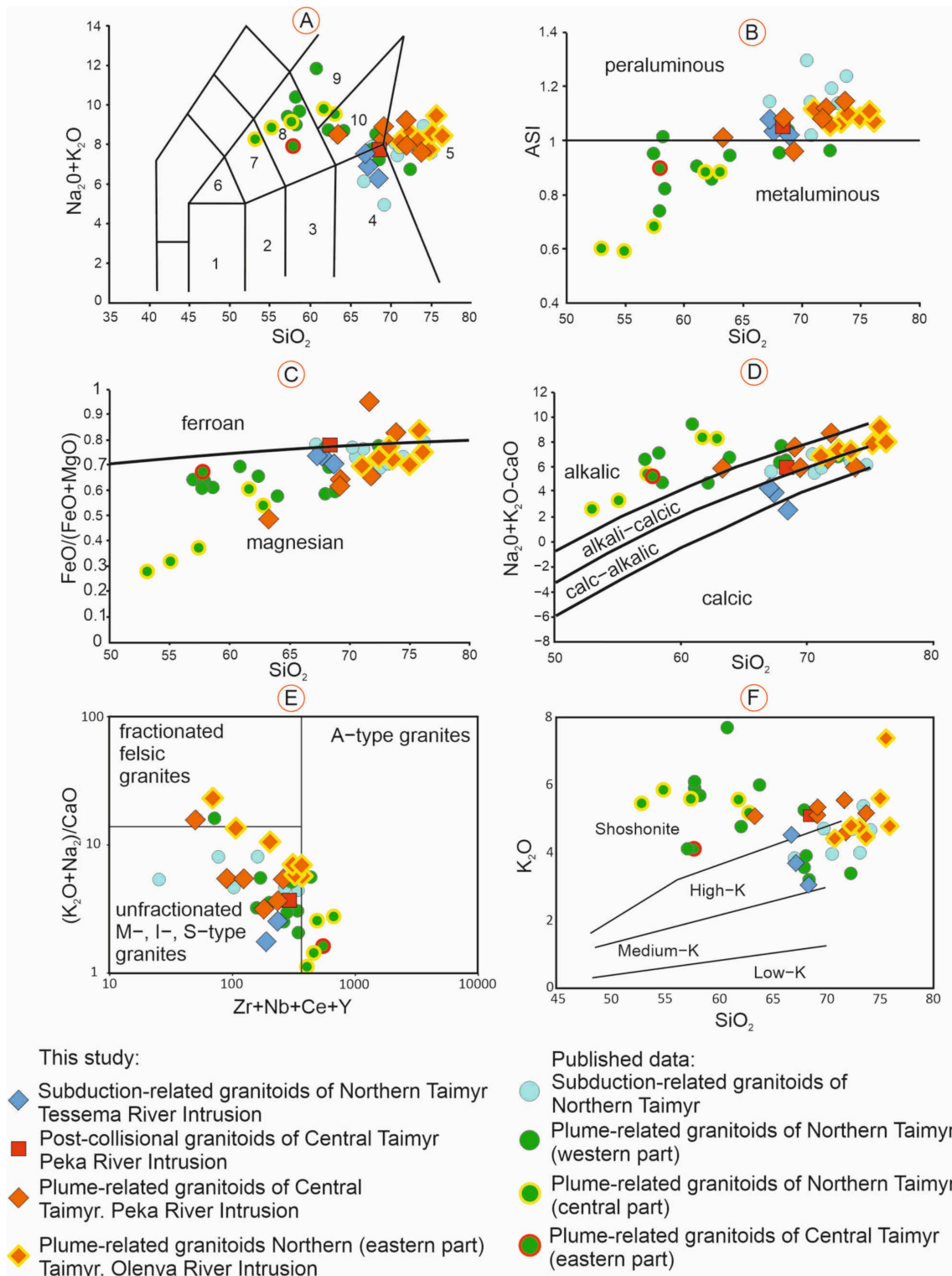


**Figure 6.** Classification diagrams for Taimyr granites. (A)  $\text{Na}_2\text{O} + \text{K}_2\text{O}$  vs.  $\text{SiO}_2$  diagram after [80]. (B) Alumina Saturation Index ( $\text{ASI} = \text{Al}_2\text{O}_3 / (\text{Na}_2\text{O} + \text{K}_2\text{O} + \text{CaO})$ ) vs.  $\text{SiO}_2$ . (C)  $\text{FeO} / (\text{FeO} + \text{MgO})$  vs.  $\text{SiO}_2$ . (D)  $\text{Na}_2\text{O} + \text{K}_2\text{O} - \text{CaO}$  vs.  $\text{SiO}_2$  diagrams after [81]. (E) A-type granite classification diagram after [82]. (F)  $\text{K}_2\text{O}$  vs.  $\text{SiO}_2$  diagram after [83]. Fields on (A): 1, gabbro; 2, gabbro-diorite; 3, diorite; 4, granodiorite; 5, granite; 6, monzogabbro; 7, monzodiorite; 8, monzonite; 9, quartz monzonite. Published data from [15,21,22,39].

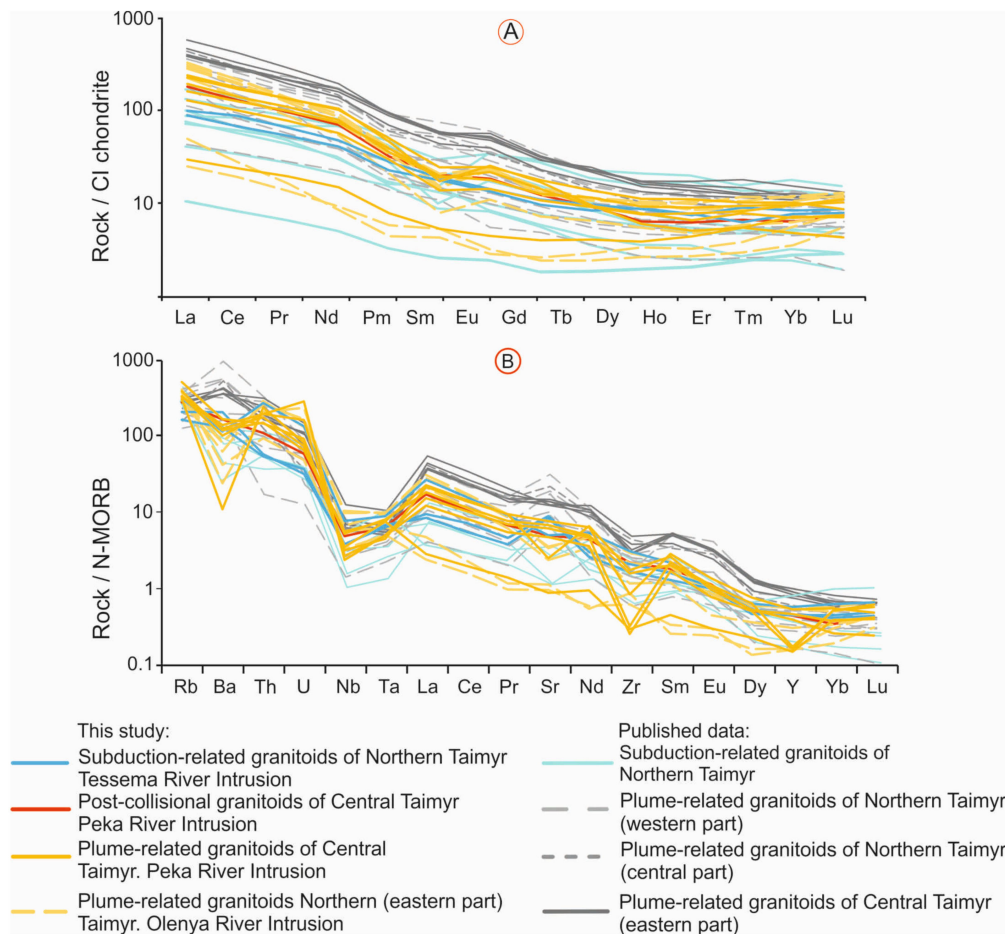


**Figure 7.** Multi-element diagrams for studied samples. (A) Chondrite-normalized REE diagram. (B) N-MORB-normalized multi-cationic diagram. Chondrite and N-MORB normalization values from [84]. Published data from [15,22,39].

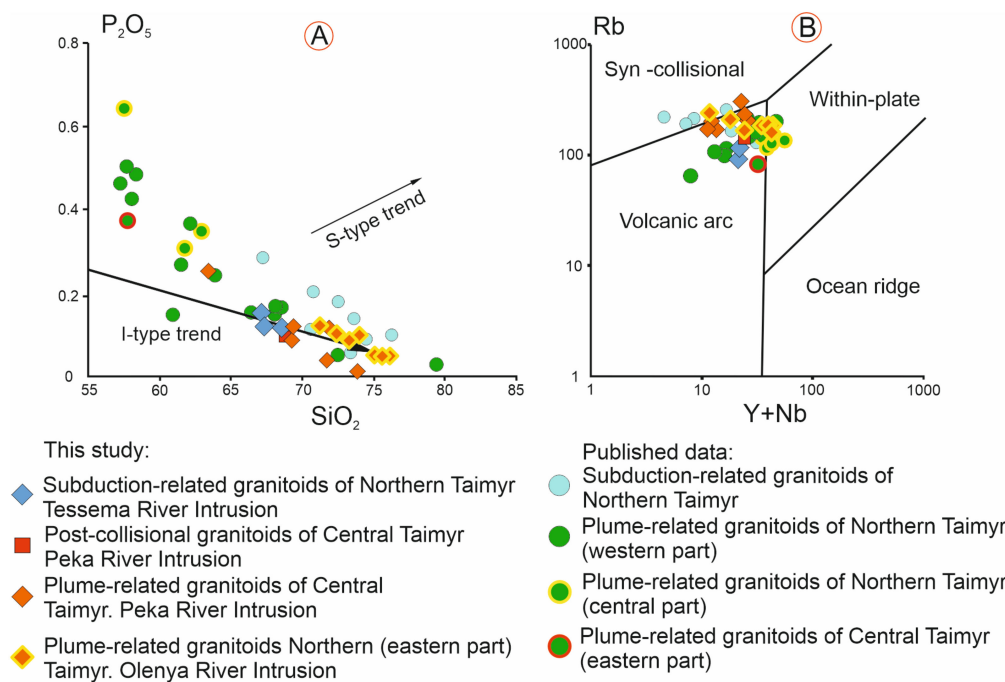


**Figure 8.** Discrimination diagrams for Taimyr granitoids. (A)  $P_2O_5$  vs.  $SiO_2$  diagram after [82]. (B) Rb vs. Y + Nb diagram after [85]. Published data from [15,22,38].

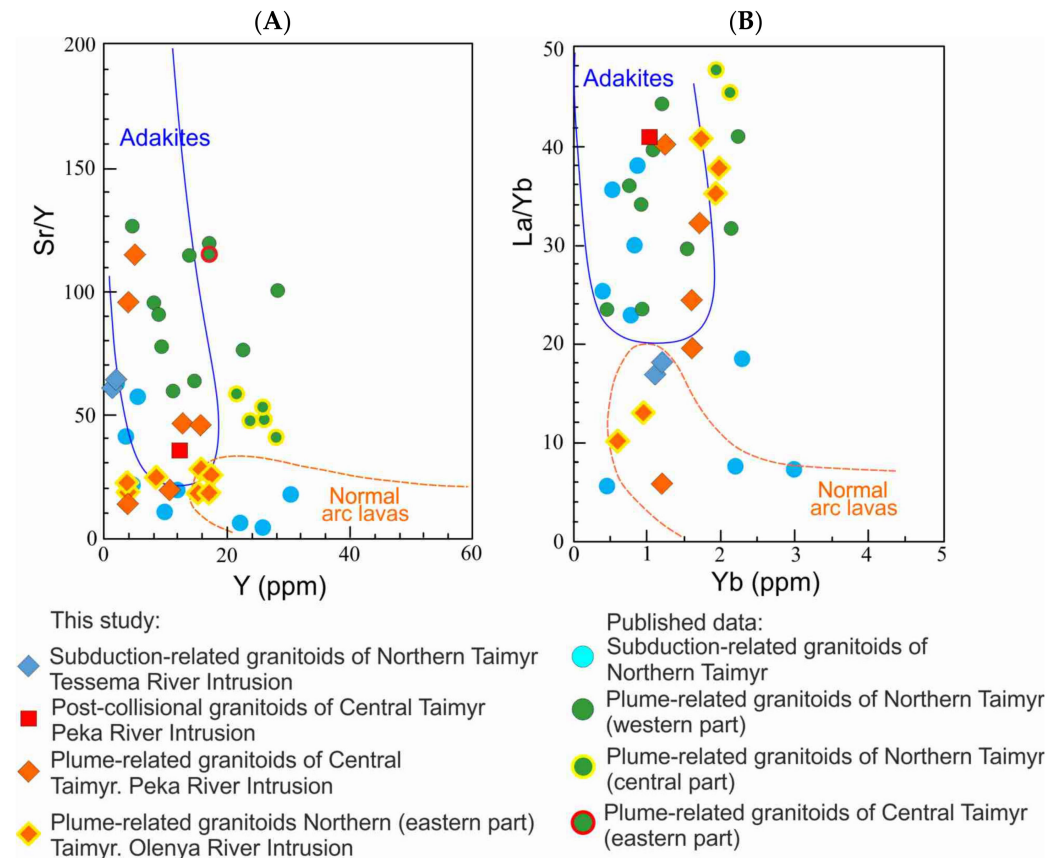


**Figure 9.** Supra-subduction, post-collisional and plume-related granitoids of Taimyr on discrimination diagrams that are used to distinguish adakite from normal arc andesite, dacite, and rhyolite lavas (after [86]). (A) Sr/Y vs. Y. (B) La/Yb vs. Yb. Field boundaries after [87]. Published data from [15,22,39].

### 6.1. Peka River Intrusion

Seven samples were collected from the Peka River intrusion. The intrusion is composed of even-grained to coarse-grained granites containing quartz (25%–30%), plagioclase (25%–28%), microcline (27%–30%), biotite (7%–10%), hornblende (2%–3%), and minor titanite, zircon, apatite, and magnetite, as well as secondary chlorite (up to 5%), sericite (up to 2%), epidote, and carbonate (Supplementary Figure S1). The analyzed samples have SiO<sub>2</sub> contents in the range of 63.3–73.7 wt.%, Na<sub>2</sub>O 2.7–3.7 wt.%, and K<sub>2</sub>O 4.6–5.5 wt.%. On the TAS classification diagram of [80], the compositions of the granitoids plot in the fields of granite and granodiorite (Figure 6A). The rocks are characterized by slightly peraluminous compositions and plot in the fields of magnesian and ferroan granites in the FeO<sub>t</sub>/(FeO<sub>t</sub> + MgO) vs. SiO<sub>2</sub> diagram of Frost et al. (2001) [81] and the fields of calc-alkaline and alkali-calcic series in the diagram (Na<sub>2</sub>O + K<sub>2</sub>O–CaO) vs. SiO<sub>2</sub> (Figure 6B–D). The REE spectra of the granites are characterized by a low to moderate enrichment in LREE and depletion in HREE (La<sub>N</sub>/Yb<sub>N</sub> = 13.2–48.8), with a pronounced negative Eu anomaly (Eu/Eu\* = 0.5–0.9) (Figure 7A). The primitive mantle-normalized multicationic diagram patterns show relative enrichment in Rb, Th, and U, and depletion in Ba, Ta, Nb, and Ti (Figure 7B).

The xenolith of rhyolite-porphyry (sample 2031/9) is moderately altered by sericitization. The content of sericite, replacing feldspars, is up to 5 vol. %. The rock contains 68.5 wt.% SiO<sub>2</sub>, 2.7 wt.% Na<sub>2</sub>O, and 5.1 wt.% K<sub>2</sub>O. The sample is alkali-calcic, as defined by the modified alkali–lime index. It is slightly peraluminous and plots on the boundary between fields of ferroan and magnesian granites (Figure 6B–D). On a Chondrite-normalized

diagram (Figure 7A), the rhyolite is characterized by a low to moderate enrichment in LREE and depletion in HREE ( $La_N/Yb_N = 27.9$ ), with a negative Eu anomaly ( $Eu/Eu^* = 0.83$ ).

### 6.2. Olenya River Intrusion

Seven samples were analyzed from the Olenya River intrusion. The sampled rocks are represented by medium-grained monzogranites with porphyritic texture containing biotite (from 3 to 5%) and amphibole (up to 2%) (Supplementary Figure S1). The analyzed samples have  $SiO_2$  contents in the range of 71.1–75.9 wt.%,  $Na_2O$  2.1–3.9 wt.%, and  $K_2O$  4.4–7.3 wt.%. The samples are classified as granites on the TAS classification diagram of [80] (Figure 6A). Samples are predominantly magnesian according to the classification of (Frost et al. 2001), alkali-calcic to calc-alkaline as defined by the modified alkali–lime index, and slightly peraluminous (Figure 6B–D). On a Chondrite-normalized diagram (Chondrite values of [84], Figure 7A), the granites are characterized by low to moderate enrichment in LREE and depletion in HREE ( $La_N/Yb_N = 7.0$ – $35.1$ ), with mainly negative Eu anomalies ( $Eu/Eu^* = 0.5$ – $1.23$ ). On an N-MORB-normalized multi-element diagram (N-MORB values of [84]), the granites are relatively enriched in Rb, Th, and U, and depleted in Ba, Ta, Nb, and Ti (Figure 7B).

### 6.3. Tessema River Intrusion

Three samples were analyzed from intrusion exposed on the left shore of the Tessema River and at the Kara Sea shore (Figure 5A,B). The intrusion is composed of relatively heterogeneous medium- to coarse-grained granodiorites containing quartz (25%–30%), plagioclase (30%–45%), microcline (12%–15%), biotite (10%–12%), hornblende (5%–7%), and minor titanite, zircon, apatite, and magnetite, as well as secondary chlorite, sericite, epidote, and carbonate (Figure 5C). Altered samples contain up to 10 vol. % of sericite (Figure 5D). The analyzed samples have  $SiO_2$  contents in the range of 67.0–68.5 wt.%,  $Na_2O$  3.1–3.4 wt.%, and  $K_2O$  3.0–4.5 wt.%. The samples are classified as granites and granodiorites on the TAS classification diagram of [80] (Figure 6A). Samples are magnesian according to the classification of (Frost et al. 2001), alkali-calcic to calc-alkaline as defined by the modified alkali–lime index, and slightly peraluminous (Figure 6B–D). On a Chondrite-normalized diagram (Chondrite values of [84], Figure 7A), the granites are characterized by a low to moderate enrichment in LREE and depletion in HREE ( $La_N/Yb_N = 11.4$ – $11.7$ ), with a negative Eu anomaly ( $Eu/Eu^* = 0.9$ – $1.0$ ). On an N-MORB-normalized multi-element diagram (N-MORB values of [84]), the granites are enriched in Rb, Th, and U, and depleted in Ba, Ta, Nb, and Ti (Figure 7B).

The studied intrusions of the Northeastern Taimyr are composed of predominantly magnesian, slightly peraluminous calc-alkaline amphibole-bearing granitoids that can be generally classified as evolved high-K I-type granites (Figure 6C–F). Berzin et al. (in press) noted that granitoids from the Peka and Tessema River intrusions had trace element composition similar to adakites [88]. Analysis of the extended geochemical dataset showed that a significant number of other Taimyr granitoids also classified as adakites using Sr/Y vs. Y and La/Yb vs. Yb discrimination diagrams (Figure 9). Thus, the adakitic geochemical signature of the Taimyr granitoids is considered as a regional feature, which is discussed below in Section 8.1.

## 7. U-Pb Zircon Geochronology

To identify the evolution of magmatism in the studied areas, we used SHRIMP-II equipment to geochronologically investigate zircon grains from seven samples collected from three intrusions. The U–Pb analytical data and calculated ages are presented in Supplementary Table S2. The CL images of representative zircon grains are shown together with the concordia diagrams in Figure 10 and in Supplementary Figure S2, and the obtained ages are incorporated in a histogram showing distribution of published intrusive ages for the whole Taimyr Peninsula (Figure 11).

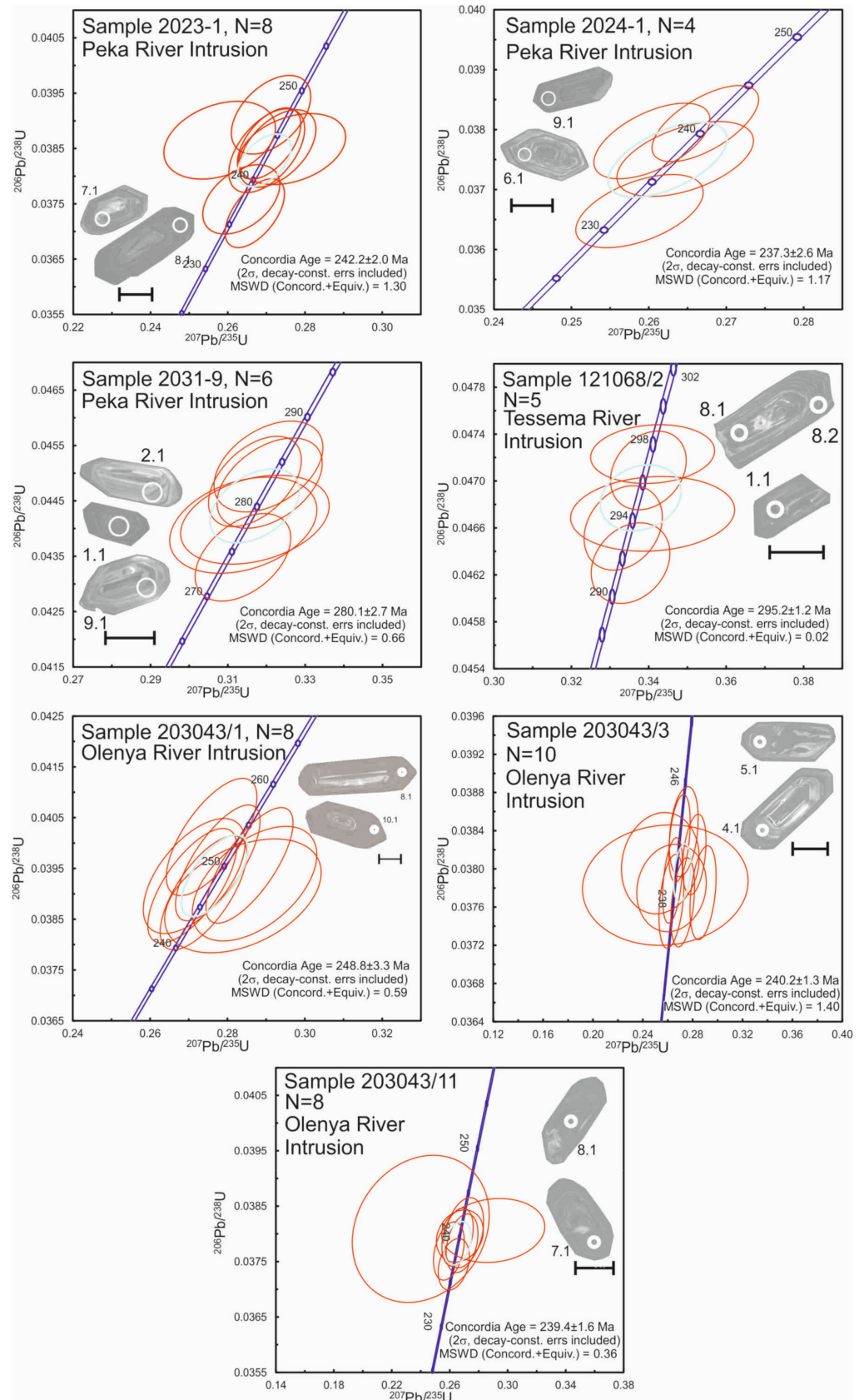


**Figure 10.** Concordia diagrams for zircon U-Pb SHRIMP data of granitoids from the Taimyr Peninsula. The scale bar on the CL images corresponds to 0.1 mm. Sample numbers as in Supplementary Table S2.

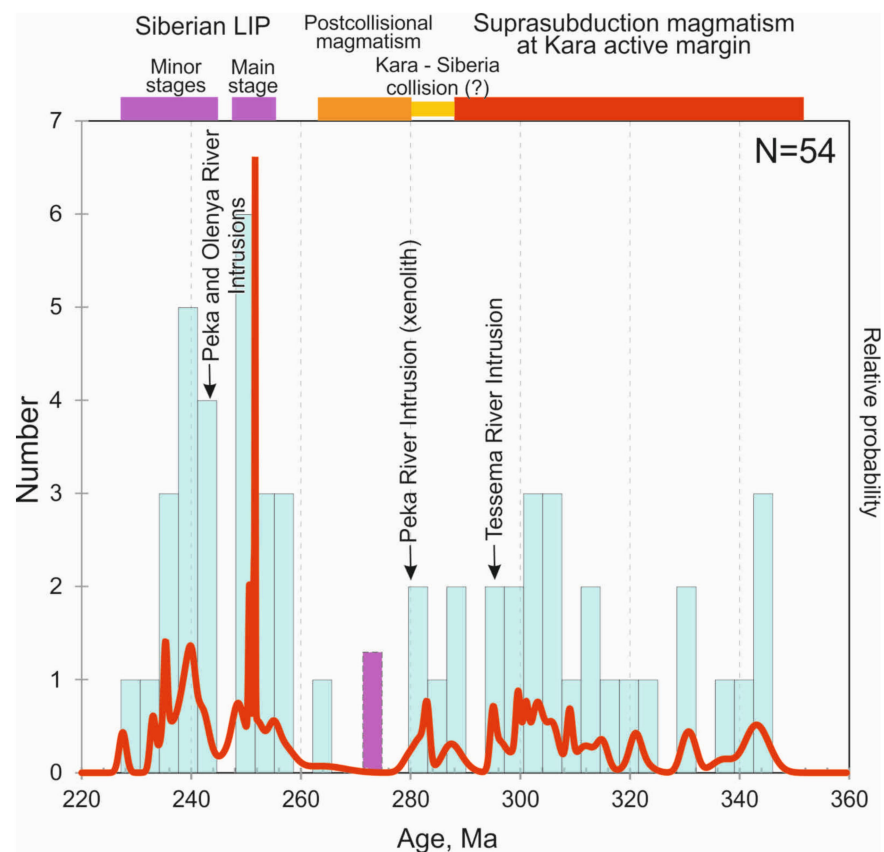


**Figure 11.** Histogram and probability density plot showing distribution of U-Pb zircon ages from granitoid intrusions of the Taimyr Peninsula. Intrusions investigated in this study are shown by arrows. Other data from [9,15,16,18,20–22,35,38–41,46]. Unpublished data by Kurapov and Proskurnin for post-collisional intrusions are shown as the lilac box and not included in the probability density plot.

### 7.1. Peka River Intrusion

Granite sample 2023/1, chosen for U-Pb zircon chronology, supplied a homogeneous population of stubby prismatic zircon grains with well-developed facets demonstrating simple oscillatory zoning and Th/U ratios in the range 0.45–1.28, characteristic for magmatic zircon. Spot analyses have been carried out on 12 grains from this sample. The U–Pb analytical data are presented in Supplementary Table S2 and on concordia diagram (Figure 10). Eight analyses plot as a tight cluster yielding a  $^{206}\text{Pb}/^{238}\text{U}$  concordia age of  $242.2 \pm 2.0$  Ma (MSWD = 1.3), which is interpreted as the crystallization age of granite sample 2023/1. Four analyses, characterized by high common Pb concentrations (0.25–1.74) pointing to metamictization, yielded slightly younger ages in the range 219–198 Ma, and were excluded from age calculation.

Zircons recovered from granite sample 2024/1 comprise a similarly homogeneous population of stubby prismatic grains, with elongation ratios varying from 1 to 4 (Figure 10), U contents from 172 to 1991 ppm, and Th/U ratios in the range 0.35–1.03 (Supplementary Table S2). Four of the 11 analyzed grains define a  $^{206}\text{Pb}/^{238}\text{U}$  concordia age of  $237.3 \pm 2.6$  Ma (MSWD = 1.17), which is a good estimate of the crystallization age of granite sample 2024/1. Four grains are slightly younger than the inferred concordia age. They are characterized by high common Pb concentration (1.31–3.43) pointing to metamictization, so these grains were not included in age calculation. Two grains are slightly older and characterized by high discordance, so they were excluded from age calculation. One grain has a Middle Permian age and most likely was inherited from a wallrock.

Granite sample 2031/9 was collected from a xenolith of presumably older age. The zircon population of sample 2031/9 is homogeneous, with elongation ratios ranging from 2 to 5 (Figure 10). U content ranges from 55 to 4319 ppm with Th/U ratios of

0.26–0.62 (Supplementary Table S2). Five of the 12 analyzed grains define a concordia age of  $280.1 \pm 2.7$  Ma (MSWD = 1.17), which constrains the crystallization age of granite sample 2024/1. Four grains are younger than the inferred concordia age. They are characterized by high common Pb concentrations (1.26–5.76) pointing to metamictization, so these grains were not included in age calculation. One grain has an older Middle Permian age and most likely it was inherited from a wallrock. This sample probably represents a fragment of an Early Permian granite body that was dismembered by a later Triassic magmatic pulse and incorporated into the Peka River intrusion as a xenolith.

### 7.2. Olenya River Intrusion

The zircon population of sample 203043/1 is homogeneous, and includes relatively large stubby prismatic zircon grains with well-developed facets demonstrating simple oscillatory zoning, with elongation ratios ranging from 2 to 5 (Figure 10). U content ranges from 376 to 1090 ppm with Th/U ratios of 0.41–0.82 (Supplementary Table S2). Eight of the 10 analyzed grains define a  $^{206}\text{Pb}/^{238}\text{U}$  concordia age of  $248.8 \pm 3.3$  Ma (MSWD = 0.59), which is a good estimate of the crystallization age of granite sample 203043/1. One grain is younger than the inferred concordia age, and characterized by high common Pb concentration (0.35 ppm) pointing to metamictization, so this grain was not included in the age calculation. One grain has a Middle Permian age and most likely was inherited from country rocks.

The zircon population of sample 203043/3 is homogeneous, and consists of stubby prismatic grains, with elongation ratios ranging from 2 to 5 (Figure 10). Some grains contain inclusions. U content ranges from 353 to 1025 ppm with Th/U ratios of 0.70–0.94 (Supplementary Table S2). All 10 analyses define a tight cluster with a  $^{206}\text{Pb}/^{238}\text{U}$  concordia age of  $240.2 \pm 1.3$  Ma (MSWD = 1.4), which is interpreted as the crystallization age of granite sample 203043/3.

The zircon population of sample 203043/11 is homogeneous, with elongation ratios ranging from 2 to 4 (Figure 10). U content ranges from 133 to 875 ppm with Th/U ratios of 0.55–2.84 (Supplementary Table S2). Eight of the ten analyzed grains define a  $^{206}\text{Pb}/^{238}\text{U}$  concordia age of  $239.4 \pm 1.6$  Ma (MSWD = 0.36), which is interpreted as the crystallization age of granite sample 203043/11. Two grains are close in age to the inferred concordia age, but characterized by high common Pb concentration (1.67–2.97 ppm) pointing to metamictization, so these grains were not included in age calculation.

### 7.3. Tessema River Intrusion

The zircon population of sample 121068/2 is heterogeneous, and includes stubby prismatic zircon grains, with well-developed facets demonstrating simple oscillatory zoning as well as angular fragments of larger grains which are dark-colored in CL images (Figure 10). Measured U content ranges from 513 to 4849 ppm with Th/U ratios of 0.30–1.84 (Supplementary Table S2). Ten zircon grains were analyzed, including both prismatic and dark-colored varieties. Nine out of 10 analyses yielded  $^{206}\text{Pb}/^{238}\text{U}$  ages in the range 296–281 Ma, and one analysis yielded a significantly younger age of 141 Ma. Five tightly clustered analyses define a  $^{206}\text{Pb}/^{238}\text{U}$  concordia age of  $295.2 \pm 1.2$  Ma (MSWD = 1.17), which is interpreted as the crystallization age of granite sample 121068/2. Four grains are slightly younger than the inferred concordia age. They are characterized by high common Pb concentration (5.63–20.93 ppm) pointing to metamictization, so these grains were excluded from age calculation.

## 8. Discussion

### 8.1. Geochronology, Geochemistry, and Petrogenesis of the Taimyr Granitoid Series

The distribution of published crystallization ages of granitoid intrusions from the Taimyr Peninsula is illustrated by a histogram and probability density plot presented in Figure 11. It is generally accepted that the Taimyr granitoid series formed in three different geodynamic settings including the Carboniferous active margin of the Kara Block, Early

Permian post-collisional environment, and Permo–Triassic intra-plate rifting associated with formation of Siberian LIP [15,35].

As seen in Figure 11, supra-subduction magmatism at the southern active margin of the Kara Block continued from ca. 345 to 285 Ma, and granitoid intrusions of this stage are localized in the Northern Taimyr Domain comprising the southern margin of the Kara Block. After the Early Permian collision of Kara with the Siberian Craton, post-collisional granitoids were emplaced in all Taimyr domains across terrane boundaries within a time span between ca. 285 and 265 Ma. After cessation of the post-collisional magmatism, at the Permo–Triassic boundary, the Taimyr experienced extension, and voluminous magmatic series associated with a Siberian mantle plume formed between 251 and 228 Ma.

Granites of the Tessema River intrusion in the Northern Taimyr Domain yielded an age of 295 Ma (Figure 10). The analyzed samples of the Tessema River granites follow the I-type trend in the  $P_2O_5$  vs.  $SiO_2$  diagram [82] (Figure 8A). They mainly plot in the fields of island arc and syn-collisional granites in the  $Y + Nb$  vs.  $Rb$  discrimination diagram of Pearce et al. (1984) [85] (Figure 8B) and demonstrate LREE-enriched patterns and negative Ta and Nb anomalies in multicationic diagrams (Figure 7). These geochemical features are also typical for granitoids from other supra-subduction intrusions of the Northern Taimyr Domain, which are shown on the corresponding diagrams for comparison. Thus, the Tessema River intrusion, together with the recently described adjacent Pervomayski Island massif [15], are interpreted to represent a supra-subduction magmatic series formed at the active southern margin of Kara Block.

Granitoid xenolith from the Triassic plume-related Peka River intrusion (sample 2031/9), located to the south of the Main Taimyr Fault in the Central Taimyr Domain, produced an Early Permian age of 280 Ma and probably represents a fragment of older granitoid body formed at post-collisional stage. Similar crosscutting relationships of Triassic granites intruding older Carboniferous and Permian granitoid massifs are common and have been described elsewhere in the Taimyr Peninsula [15,22]. An age of 280 Ma obtained for post-collisional granite, located in the Central Taimyr Domain, which is interpreted as a former passive margin of the Siberian Craton, may indicate that the Kara Block had already been accreted to Siberia by the Early Permian.

Granite samples from the Olenya River intrusion, located in the Northern Taimyr Domain, yielded Early–Middle Triassic ages in the range 249–239 Ma, typical for Siberian plume-related intrusions. Two samples from the Peka River intrusion located in the Central Taimyr Domain yielded similar Middle Triassic ages of 242 and 237 Ma, representing the easternmost Triassic granite dated in Taimyr so far. The granites from both intrusions are marginally peraluminous and plot in the fields of volcanic arc and syn-collisional granites and in the  $Rb$  vs.  $Y + Nb$  discrimination diagram (Figures 6 and 8). These geochemical characteristics are typical for granitoids from Triassic plume-related intrusions elsewhere in the Taimyr Peninsula [20,22,39].

The granitoid series of the Taimyr Peninsula formed in different geodynamic settings during a time span of almost 100 Ma. However, despite their diverse origin, most of the Taimyr granitoids demonstrate geochemical characteristics typical for granites of active continental margins (Figures 6–8). Although Triassic plume-related granites of the Taimyr formed in the intra-plate tectonic environment, they generally inherit the geochemical features of supra-subduction granitoids and can be classified as evolved high-K I-type granites (Figure 6E). Shoshonitic affinities of the plume-related granitoids from the Western Taimyr, illustrated in Figure 6F, were recently described by Proskurnina et al. [39].

Berzin et al. (in press) have shown that granitoids from the Peka and Tessema River intrusions had pronounced geochemical affinity to adakites, and additional analysis of the extended geochemical dataset has revealed that a significant number of other Taimyr plume-related granitoids also classified as adakites utilizing  $Sr/Y$  vs.  $Y$  and  $La/Yb$  vs.  $Yb$  discrimination diagrams (Figure 9).

The term “adakite” was introduced by Defant and Drummond (1990) [86] to describe intermediate-felsic igneous rocks from Adak Island in the Aleutian arc, in which major

and trace element composition suggested an origin by melting of subducted basaltic crust. Adakites are silica- ( $\text{SiO}_2 > 56$  wt.%) and sodium-rich ( $\text{K}_2\text{O}/\text{Na}_2\text{O} < 0.5$ ) rocks with high Sr ( $\geq 400$  ppm) and low Y ( $\leq 18$  ppm) and Yb ( $\leq 1.9$  ppm) concentrations, and high Sr/Y ( $> 40$ ) and La/Yb ( $> 20$ ) ratios [86,87,89]. In recent decades,  $\text{K}_2\text{O}$ -rich igneous rocks with adakitic trace element composition have been widely reported from post-collisional settings, such as in Tibet after 50 Ma, and described as high potassium continental adakites [48,50,90]. Adakitic granitoids, identified in the Taimyr Peninsula, have  $\text{K}_2\text{O}/\text{Na}_2\text{O}$  ratios in the range 0.3–6.9 (Supplementary Table S1) and generally plot in the field of shoshonitic series in the  $\text{K}_2\text{O}$  vs.  $\text{SiO}_2$  diagram (Figure 6F), and, thus, are similar to high potassium continental adakites characteristic for post-collisional settings.

Sodium-rich adakites are commonly considered to be generated by partial melting of MORB at eclogite facies [91], while potassium-rich continental adakites are generally attributed to partial melting of thickened and/or hydrated mafic lower crust [92]. Experimental studies using hydrated mafic lower crust as starting materials show that the adakitic signature is not necessarily a result of anatexis at eclogite facies conditions. It was proved that the source rock lithological compositions, and especially fluid contents, are also critical because the geochemical signatures of adakitic melts are mainly controlled by residual minerals [93,94].

The leading role of the source lithology probably can explain the geochemical features of the granitoid series of the Taimyr Peninsula where granites with similar adakitic and I-type affinities were repeatedly generated in supra-subduction, post-collisional, and plume-related tectonic settings during the time span of almost 50–70 million years. The geochemical connection between supra-subduction and plume-related granitoids of the Taimyr Peninsula is also illustrated by Nd and Sr isotopic compositions of these rocks. In a diagram  $\epsilon\text{Nd}$  vs.  $^{87}\text{Sr}/^{86}\text{Sr}$ , presented in Figure 12, both granitoid series generally plot in the field of Siberian traps and demonstrate variably mixed Nd-Sr isotopic signatures typical for the continental arc environment where mantle-derived magmas interact with continental crust.

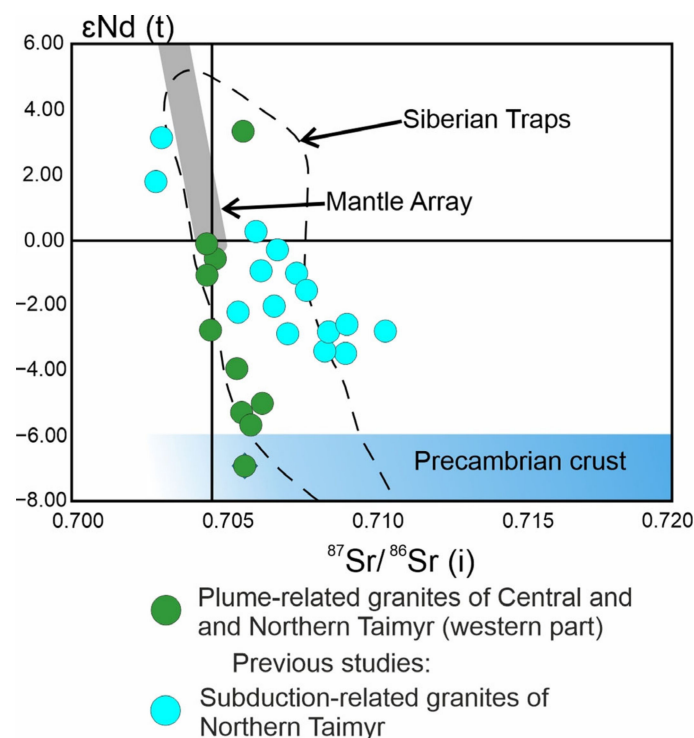


**Figure 12.** Initial  $\epsilon\text{Nd}$  vs.  $^{87}\text{Sr}/^{86}\text{Sr}$  diagram for granitoids from the Taimyr Peninsula (data from [15,21,22]). Reference fields for mantle and Proterozoic crust are shown for orientation (data from [95–98]). Field of Siberian traps is given for comparison after [99].

Thus, it can be tentatively suggested that adakitic granitoids of the Taimyr Peninsula were produced by melting of hydrated mafic lower crustal protholiths in post-collisional and intra-plate tectonic settings, and their adakitic geochemical signatures were probably controlled by the source lithology and fluid content.

#### *8.2. Late Paleozoic–Early Mesozoic Tectono-Magmatic Evolution of the Taimyr–Severnaya Zemlya Fold-and-Thrust Belt*

An eye-catching feature of the Main Taimyr fault zone, which represents an inferred collisional suture between the Kara Block and Siberia, is a lack of Paleozoic ophiolites, oceanic sediments, and UHP metamorphic rocks that are typical for similar collisional zones in coeval Hercynian orogenic belts of the Urals [100,101] and South Tien-Shan [102–104]. It is suggested that these formations could be destroyed by collisional tectonics, possible mechanisms of which are discussed below. Therefore, the Late Paleozoic magmatic series comprise nearly the only evidence of convergence between Siberia and Kara preserved in the geological record.

Supra-subduction granitoid intrusions in the Northern Taimyr Domain, making up the southern part of the Kara Block, have ages in the range from ca. 345 Ma, corresponding to the Middle Carboniferous (Visean), to ca. 280 Ma, corresponding to the Early Permian (Figure 11). This time span of ca. 40–50 Ma matches well with the duration of episodes of supra-subduction magmatism reported for other Hercynian active margins and elsewhere (e.g., [105]). Formation of supra-subduction intrusions in the southern part of the Kara Block is illustrated in the geodynamic reconstruction shown in Figure 13A for a time slice of 345–295 Ma.

The timing of collision between the Siberian and Kara continents is rather difficult to constrain due to significant syn- and post-collisional deformations and subsequent tectonic erosion. The distribution of crystallization ages shows that supra-subduction Carboniferous magmatism was followed, without interruption in time, by the emplacement of the Early Permian post-collisional complexes that also inherited geochemical signatures of subduction-related granitoids, which is typical for active continental margins elsewhere (e.g., [106]) (Figure 11). Therefore, the evidence for the timing of post-collisional uplift comes from the geological record preserved in the sedimentary sequences of the Yenisei–Khatanga paleo-rift, where the Lower Permian (Asselian) siltstones of the Turuzov and Falabigai formations change in their upsection to overlying sandy layers of the Byrrang Formation, for which the sandy material was clearly sourced from the rising collisional belt of the Taimyr [69,107,108]. This supports known reconstructions of collisional events during the Asselian stage of the Lower Permian and is in accordance with the ages of post-collisional granites that appear in the Central Taimyr Domain after ca. 280 Ma, probably due to slab break-off as shown in the geodynamic reconstruction given in Figure 13B for the time slice of 287–280 Ma. Additional evidence that the Kara Block had already been accreted to Central Taimyr Domain by the Early Permian is provided by an age of 280 Ma obtained for a granite xenolith in the Peka River intrusion, located in the Central Taimyr Domain, in this study.

Based on the large set of data, it was suggested that a transform fault existed between the Siberian and Kara continents as early as the Early Permian, and this structure was turned into a series of large-amplitude longitudinal sinistral shear zones at the post-collisional stage due to the oblique character of the collision and significant clockwise rotation of Siberia [35,109] (Figure 2). These deformations might be responsible for the destruction of the accretionary wedge as a result of tectonic erosion and explain the absence of the ophiolites along the Main Taimyr fault. After the collision, the region experienced uplift and erosion that was constrained by metamorphic ages [15] and thermochronological studies [22]. Cessation of post-collisional magmatism took place at ca. 265 Ma (Figure 11).

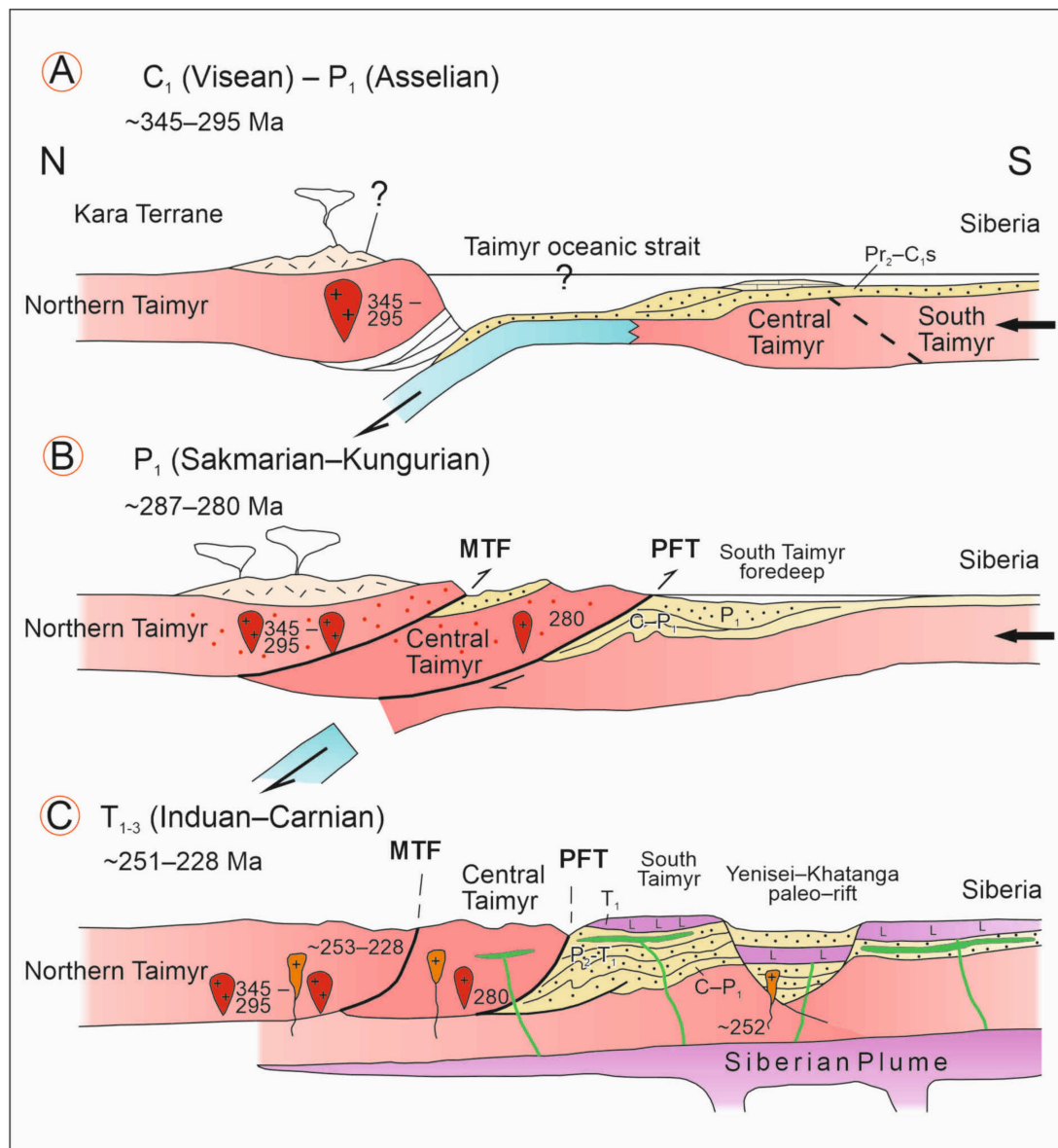


**Figure 13.** Geodynamic setting and tectonic evolution of the Kara Block and Siberian Craton in the Late Paleozoic–Early Mesozoic. (A) Reconstruction for Early Carboniferous (Visean)–Early Permian (Asselian). Passive margin of Siberia and the Kara Block are separated by inferred oceanic basin with subduction to the north under the Kara continental margin, where supra-subduction magmatic series are shown. (B) Reconstruction for Early Permian (Sakmarian–Kungurian). Collision of Kara with Siberia followed by crustal thickening, metamorphism, post-collisional magmatism, and uplift of Northern and Central Taimyr domains. The Southern Taimyr foredeep is superimposed on the Siberian passive margin. (C) Reconstruction for Early–Late Triassic showing the influence of Siberian plume manifested by crustal extension and formation of plume-related bimodal magmatic series. Abbreviations: MTF—Main Taimyr Fault, PFT—Piasina–Faddey Thrust.

At the Permo–Triassic boundary, one of the largest LIPs in Earth history formed in the northwestern part of Siberia as a result of a Siberian mantle plume that was presumably centred approximately 1000 km to the SSW of Taimyr [27,32,72,110] (Figure 1B). This event triggered emplacement of plume-related intrusions all over the Taimyr Peninsula and was well documented in the geological record preserved in the sedimentary sequences of the Yenisei–Khatanga paleo-rift [111]. The latter originally formed as a Middle Carboniferous–Early Permian foredeep superimposed on the Siberian margin as a result of

ongoing Hercynian collision with the Kara Block (Figure 13B). However, after collision, the subsidence in the Yenisei–Khatanga trough resumed at the Permo–Triassic boundary due to Siberian plume-related extension and under the load of erupted volcanic rocks reaching up to 2000 m in thickness in the Southern Taimyr Domain [112]. An age of 248 Ma reported for basalt flow from the Southern Taimyr Domain corresponds to the peak of plume-related magmatism elsewhere in Siberia [112], and overlaps with 252–248 Ma ages of granitoid intrusions associated with the main plume-related magmatic pulse in the Taimyr Peninsula (Figures 11 and 13C). The plume-related granitoid magmatism in Taimyr continued for ca. 20–25 Ma, until the Upper Triassic, and included several minor pulses between 241 and 230 Ma [32,112–115], with the youngest intrusions dated at 229–228 Ma [116] (Figure 11). On a regional scale, this Triassic tectono-magmatic evolution established for the Taimyr Peninsula enables a better understanding of the geodynamic setting of the less studied Triassic granites known in adjacent tectonic areas of the Polar Urals and Novosibirsk Block [117,118]. Furthermore, the magmatic episodes recognized in the Taimyr Peninsula are also well documented in age spectra of detrital zircon grains from the Mesozoic sedimentary rocks covering the northeastern part of the Siberian Craton [119–121].

### 8.3. Implications for Tectonic Evolution of the Arctic Continental Margins

In early paleo-tectonic reconstructions, it was supposed that in the Middle Paleozoic, the Kara Block was part of a hypothetical continent, Arctida [55], or developed as an individual microcontinent [57]. However, recent works, based on new geochronological and seismic data, have shown that in the Middle Paleozoic, the Kara Block was probably incorporated in a post-Ediacaran continental terrane formed at the northern margin of Baltica as a result of Timanian orogeny [54,56]. This is supported by “Timanian” age spectra of detrital zircon grains recovered from the Kara basement [54,64,122] and by the absence of Cambrian carbonate sediments in the Kara Block, which is ubiquitously typical of eastern European parts of Baltica, in contrast to Siberia where abundant Cambrian limestones were deposited in a warmer climate. However, the Late Paleozoic evolution paths of Kara and Baltica differ significantly. The Eastern (Uralian) margin of Baltica developed as a passive margin until the Early Permian collision, while its inferred continuation in the Kara Block turned into an active margin in the Early Carboniferous (Visean). In order to resolve this controversy, several authors have suggested that large-amplitude dextral displacement of the Kara Block relative to Baltica took place in the Early Carboniferous and was later accommodated by formation of a collisional belt in the Northern Taimyr [1,58] (Figure 2). This suggestion can be tested when more data on the geological structure of the submerged northern part of the Kara Block are obtained. Similarly, additional research and detailed remote sensing data are needed to decipher the eastern continuation of the Taimyr structures and their junction with the Novosibirsk Block under the Laptev Sea shelf sediments (Figure 1). In this area, the Early Paleozoic detrital zircon grains, supposedly derived from the Caledonian orogenic belt at northern Baltica margins, were recently reported from Devonian–Carboniferous sediments outcropping in Kotelny Is. in the central part of the Novosibirsk Block [122]. This may point to possible connection between the Novosibirsk and Svalbard blocks during the Middle Paleozoic and suggests that concurrent large-amplitude transform displacement of the Kara Block along the Siberian margin took place in the Middle–Late Paleozoic times.

After Hercynian collision, the Taimyr was incorporated in the northern Eurasian margin as an uplifted block that was affected by Siberian plume-related magmatism at the Permo–Triassic boundary. Although the Taimyr was located at the periphery of the plume, centered ca. 1500 km to the south (Figure 1B), the presence of grabens filled with Triassic clastic sediments in the Southern Taimyr [17,18] shows that the lithosphere of this domain experienced plume-related extension, a process that was also registered elsewhere in adjacent Arctic continental margins [23–25]. Triassic sedimentary fill of the grabens was derived from the Northern Taimyr domains that underwent surface erosion and provided clastic material in surrounding basins. Recent studies [123,124] have shown that age spectra

of detrital zircon grains, recovered from Jurassic sediments of the Canada basin and North American shelf, demonstrate major Devonian–Early Carboniferous peaks sourced from the rocks of the Ellesmerian orogenic cycle, and several additional peaks ranging from Middle Carboniferous to Late Triassic. The latter may be explained by the erosion of the Taimyr–Severnaya Zemlya terranes supplying clastic material to the easternmost parts of Canadian shelf, such as the Sverdrup basin separating the northern part of Greenland from Canada [123,124] (Figure 1).

## 9. Conclusions

The ages of three granitoid intrusions located in the Northeastern Taimyr Peninsula have been established by ion microprobe zircon dating. The granite sample from the Tessema River intrusion, located in the Northern Taimyr Domain, yielded an Early Permian age of 295 Ma, which is typical for supra-subduction intrusions elsewhere in the Northern Taimyr. Three samples from the Olenya River intrusion, also located in Northern Taimyr, yielded Early–Middle Triassic ages in the range 249–239 Ma, typical for Siberian plume-related intrusions. Two samples from the Peka River intrusion, located in the Central Taimyr Domain, yielded similar Middle Triassic ages of 242 and 237 Ma, representing the easternmost Triassic granite dated in Taimyr so far, and one sample from granitic xenolith from this intrusion produced an Early Permian age of 280 Ma.

Geochronological data show that supra-subduction magmatism at the southern active margin of the Kara Block continued from ca. 345 to 285 Ma and was followed by a post-collisional magmatic pulse at ca. 280 Ma. An age of 280 Ma obtained for a granite xenolith in the Peka River intrusion, located in the Central Taimyr Domain, may indicate that the Kara Block had already been accreted to the Central Taimyr Domain by the Early Permian. After cessation of the post-collisional magmatism at ca. 265 Ma, the Taimyr experienced extension, and voluminous magmatic series associated with a Siberian mantle plume have been formed within a time span between 251 and 228 Ma. A Middle Triassic age, identified in this study for the Peka River intrusion, shows that Siberian plume-related granitoid magmatism was manifested as far as the northeastern edge of the Taimyr Peninsula.

The studied post-collisional and plume-related intrusions of the Northeastern Taimyr are generally classified as evolved high-K I-type granites with adakitic affinity. It is suggested that adakitic geochemical characteristics of plume-related granitoids resulted from melting of hydrated mafic lower crustal protoliths and were probably controlled by the source lithology.

**Supplementary Materials:** The following are available online at <https://www.mdpi.com/article/10.3390/min14040423/s1>. Supplementary Table S1: Geochemical data and sample coordinates for the Taimyr granitoid intrusions. Supplementary Table S2: U-Pb analytical data and calculated ages for the Taimyr granitoid intrusions. Supplementary Figure S1: photomicrographs of granitoids from Peka and Olenya river intrusions. Supplementary Figure S2: BSE and CL-images of the studied zircon grains.

**Author Contributions:** Conceptualization, M.Y.K., D.L.K. and Y.S.B.; formal analysis, M.Y.K., D.L.K. and Y.S.B.; funding acquisition, D.L.K.; investigation, M.Y.K., V.F.P., S.V.P., M.A.P., S.V.B., V.B.E., Y.Y.B. and S.Y.S.; methodology, M.Y.K., V.F.P., S.V.P., M.A.P. and S.V.B.; resources, S.V.P. and M.A.P.; supervision, D.L.K., Y.S.B. and S.V.P.; visualization, M.Y.K. and D.L.K.; writing—original draft, M.Y.K., D.L.K. and Y.S.B.; writing—review & editing, M.Y.K., D.L.K. and Y.S.B. All authors have read and agreed to the published version of the manuscript.

**Funding:** This work was supported by the Russian Science Foundation, Project # 23-27-00283 to M.Y.K., D.L.K., S.V.P. and S.V.B.

**Data Availability Statement:** Data are contained within the article and Supplementary Materials.

**Acknowledgments:** We are indebted to many colleagues for their help and cooperation during field work in Taimyr and at the stage of laboratory studies. We are very grateful for detailed and constructive comments by Michel Villeneuve and three anonymous reviewers that helped to improve the original version of the manuscript.

**Conflicts of Interest:** The authors declare no conflicts of interest.

## References

1. Nikishin, A.M.; Petrov, V.I.; Startseva, K.F.; Rodina, E.A.; Posmentier, H.W.; Foulger, G.R.; Glumov, I.F.; Morozov, A.F.; Verzhbitsky, V.E.; Malyshev, N.A.; et al. *Seismostratigraphy, Paleogeography and Paleotectonics of the Arctic Deep-Water Basin and Its Russian Shelf*, 632nd ed.; GIN RAS: Moscow, Russia, 2022.
2. Moran, K.; Backman, J.; Brinkhuis, H.; Clemens, S.C.; Cronin, T.; Dickens, G.R.; Eynaud, F.; Gattacceca, J.; Jakobsson, M.; Jordan, R.W.; et al. The Cenozoic Palaeoenvironment of the Arctic Ocean. *Nature* **2006**, *441*, 601–605. [[CrossRef](#)] [[PubMed](#)]
3. Golonka, J. Chapter 6: Phanerozoic Palaeoenvironment and Palaeolithofacies Maps of the Arctic Region. *Geol. Soc. Mem.* **2011**, *35*, 79–129. [[CrossRef](#)]
4. Martinez, N.C.; Murray, R.W.; Dickens, G.R.; Kölling, M. Discrimination of Sources of Terrigenous Sediment Deposited in the Central Arctic Ocean through the Cenozoic. *Paleoceanography* **2009**, *24*, 1–3. [[CrossRef](#)]
5. Gee, D.G.; Bogolepova, O.K.; Lorenz, H. The Timanide, Caledonide and Uralide Orogens in the Eurasian High Arctic, and Relationships to the Palaeo-Continents Laurentia, Baltica and Siberia. *Geol. Soc. Mem.* **2006**, *32*, 507–520. [[CrossRef](#)]
6. Amato, J.M.; Aleinikoff, J.N.; Akinin, V.V.; McClelland, W.C.; Toro, J. Age, Chemistry, and Correlations of Neoproterozoic-Devonian Igneous Rocks of the Arctic Alaska-Chukotka Terrane: An Overview with New U-Pb Ages. *Spec. Pap. Geol. Soc. Am.* **2014**, *506*, 29–57. [[CrossRef](#)]
7. Vernikovskiy, V.A.; Dobretsov, N.L.; Metelkin, D.V.; Matushkin, N.Y.; Koulakov, I.Y. Concerning Tectonics and the Tectonic Evolution of the Arctic. *Russ. Geol. Geophys.* **2013**, *54*, 838–858. [[CrossRef](#)]
8. Augland, L.E.; Andresen, A.; Corfu, F.; Daviknes, H.K. Late Ordovician to Silurian Ensialic Magmatism in Liverpool Land, East Greenland: New Evidence Extending the Northeastern Branch of the Continental Laurentian Magmatic Arc. *Geol. Mag.* **2012**, *149*, 561–577. [[CrossRef](#)]
9. Kurapov, M.Y.; Ershova, V.B.; Khudoley, A.K.; Makariev, A.A.; Makarieva, E.M. The First Evidence of Late Ordovician Magmatism of the October Revolution Island (Severnaya Zemlya Archipelago, Russian High Arctic): Geochronology, Geochemistry and Geodynamic Settings. *Nor. J. Geol.* **2020**, *100*, 1–15. [[CrossRef](#)]
10. Corfu, F.; Andersen, T.B.; Gasser, D. The Scandinavian Caledonides: Main Features, Conceptual Advances and Critical Questions. *Geol. Soc. Spec. Publ.* **2014**, *390*, 9–43. [[CrossRef](#)]
11. Lorenz, H.; Männik, P.; Gee, D.G.; Proskurnin, V.F. Geology of the Severnaya Zemlya Archipelago and the North Kara Terrane in the Russian High Arctic. *Int. J. Earth Sci.* **2008**, *97*, 519–547. [[CrossRef](#)]
12. Proskurnin, V.F. New Volcano-Plutonic Association of Severnaya Zemlya and Features of Its Metal Content. In *Taimyr Subsoil*; VSEGEI: Norilsk, Russia, 1995; Volume 1, pp. 93–100.
13. Proskurnin, V.F. On the Issue of Angular Unconformities in the Upper Precambrian and Lower Paleozoic of the Severnaya Zemlya Archipelago. In *Taimyr Subsoil*; VSEGEI: Norilsk, Russia, 1999; pp. 68–76.
14. Luchitskaya, M.V.; Sokolov, S.D.; Kotov, A.B.; Natapov, L.M.; Belousova, E.A.; Katkov, S.M. Late Paleozoic Granitic Rocks of the Chukchi Peninsula: Composition and Location in the Structure of the Russian Arctic. *Geotectonics* **2015**, *49*, 243–268. [[CrossRef](#)]
15. Kurapov, M.Y.; Ershova, V.B.; Khudoley, A.; Luchitskaya, M.V.; Makariev, A.A.; Makarieva, E.M.; Vishnevskaya, I.A. Late Palaeozoic Magmatism of Northern Taimyr: New Insights into the Tectonic Evolution of the Russian High Arctic. *Int. Geol. Rev.* **2020**, *63*, 1990–2012. [[CrossRef](#)]
16. Kurapov, M.Y.; Ershova, V.B.; Makariev, A.A.; Makarieva, E.V.; Khudoley, A.K.; Luchitskaya, M.V.; Prokopiev, A.V. Carboniferous Granitoid Magmatism of Northern Taimyr: Results of Isotopic-Geochemical Study and Geodynamic Interpretation. *Geotectonics* **2018**, *52*, 225–239. [[CrossRef](#)]
17. Pogrebitsky, Y. *Paleotectonical Analysis of the Taimyr Fold System*; Nedra: Leningrad, Russia, 1971.
18. Vernikovskiy, V.A. The Geodynamic Evolution of the Taimyr Folded Area. *Geol. Pac. Ocean* **1996**, *12*, 691–704.
19. Bezzubtsev, V.V.; Zalyaleyev, R.M.; Sakovich, A.B. *Geological Map of Mountainous Taimyr 1:500 000: Explanatory Notes*; Krasnoyarskgeologia: Krasnoyarsk, Russia, 1986.
20. Augland, L.E.; Ryabov, V.V.; Vernikovskiy, V.A.; Planke, S.; Polozov, A.G.; Callegaro, S.; Jerram, D.A.; Svensen, H.H. The Main Pulse of the Siberian Traps Expanded in Size and Composition. *Sci. Rep.* **2019**, *9*, 18723. [[CrossRef](#)] [[PubMed](#)]
21. Vernikovskiy, V.A.; Pease, V.L.; Vernikovskaya, A.E.; Romanov, A.P.; Gee, D.G.; Travin, A.V. First Report of Early Triassic A-Type Granite and Syenite Intrusions from Taimyr: Product of the Northern Eurasian Superplume? *Lithos* **2003**, *66*, 23–36. [[CrossRef](#)]
22. Kurapov, M.Y.; Ershova, V.B.; Khudoley, A.K.; Luchitskaya, M.V.; Stockli, D.F.; Makariev, A.A.; Makarieva, E.M.; Vishnevskaya, I.A. Latest Permian–Triassic Magmatism of the Taimyr Peninsula: New Evidence for a Connection to the Siberian Traps Large Igneous Province. *Geosphere* **2021**, *17*, 2062–2077. [[CrossRef](#)]
23. Vakar, V.A. Trap Formations of Taimyr. In *Petrography of Eastern Siberia*; Nauka: Moscow, Russia, 1962; pp. 256–340.
24. Dodin, D. *Metallogeny of the Taimyr-Norilsk Region (North Central Siberia)*; Nauka: Saint-Petersburg, Russia, 2002.
25. Dobretsov, N.L. Large Igneous Provinces of Asia (250 Ma): Siberian and Emeishan Traps (Plateau Basalts) and Associated Granitoids. *Geol. Geofiz.* **2005**, *46*, 870–890.
26. Senger, K.; Tveranger, J.; Ogata, K.; Braathen, A.; Planke, S. Late Mesozoic Magmatism in Svalbard: A Review. *Earth-Sci. Rev.* **2014**, *139*, 123–144. [[CrossRef](#)]
27. Ernst, R.E. *Large Igneous Provinces*; Cambridge University Press: Cambridge, MA, USA, 2014; ISBN 9781139025300.

28. Maher, J. Manifestations of the Cretaceous High Arctic Large Igneous Province in Svalbard. *J. Geol.* **2001**, *109*, 91–104. [[CrossRef](#)]
29. Kristoffersen, Y.; Nilsen, E.H.; Hall, J.K. The High Arctic Large Igneous Province: First Seismic-Stratigraphic Evidence for Multiple Mesozoic Volcanic Pulses on the Lomonosov Ridge, Central Arctic Ocean. *J. Geol. Soc.* **2023**, *180*, jgs2022-153. [[CrossRef](#)]
30. Dobretsov, N.L.; Vernikovskiy, V.A.; Karyakin, Y.V.; Korago, E.A.; Simonov, V.A. Mesozoic-Cenozoic Volcanism and Geodynamic Events in the Central and Eastern Arctic. *Russ. Geol. Geophys.* **2013**, *54*, 874–887. [[CrossRef](#)]
31. Harrison, J.C.; St-Onge, M.R.; Petrov, O.V.; Strel'nikov, S.I.; Lopatin, B.G.; Wilson, F.H.; Tella, S.; Paul, D.; Lynds, T.L.; Shokalsky, S.P.; et al. *Geological Map of the Arctic*; Geological Survey of Canada: Ottawa, ON, Canada, 2011.
32. Reichow, M.K.; Pringle, M.S.; Al'Mukhamedov, A.I.; Allen, M.B.; Andreichev, V.L.; Buslov, M.M.; Davies, C.E.; Fedoseev, G.S.; Fitton, J.G.; Inger, S.; et al. The Timing and Extent of the Eruption of the Siberian Traps Large Igneous Province: Implications for the End-Permian Environmental Crisis. *Earth Planet. Sci. Lett.* **2009**, *277*, 9–20. [[CrossRef](#)]
33. Vernikovskiy, V.A.; Metelkin, D.V.; Vernikovskaya, A.E.; Matushkin, N.Y.; Lobkovskiy, L.I.; Shipilov, E.V. Early Evolution Stages of the Arctic Margins (Neoproterozoic-Paleozoic) and Plate Reconstructions. In Proceedings of the ICAM VI: International Conference on Arctic Margins VI, Fairbanks, AK, USA, 30 May–2 June 2011; pp. 265–285.
34. Pease, V.; Drachev, S.; Stephenson, R.; Zhang, X. Arctic Lithosphere—A Review. *Tectonophysics* **2014**, *628*, 1–25. [[CrossRef](#)]
35. Vernikovskiy, V.A.; Vernikovskaya, A.E.; Proskurnin, V.F.; Matushkin, N.Y.; Proskurnina, M.A.; Kadilnikov, P.; Larionov, A.N.; Travin, A.V. Late Paleozoic–Early Mesozoic Granite Magmatism on the Arctic Margin of the Siberian Craton during the Kara-Siberia Oblique Collision and Plume Events. *Minerals* **2020**, *10*, 571. [[CrossRef](#)]
36. Vernikovskiy, V.A.; Neimark, L.A.; Ponomarchuk, V.A.; Vernikovskaya, A.E.; Kireev, A.D.; Kuz'min, D.S. Geochemistry and Age of Collision: Granitoides and Metamorphites of the Kara Microcontinent (Northern Taimyr). *Russ. Geol. Geophys.* **1995**, *36*, 46–60.
37. Vernikovskiy, V.A.; Sal'nikova, E.B.; Kotov, A.B.; Kovach, V.P.; Yakovleva, S.Z. Precambrian Granites of the Faddeevsky Terrane (Northern Taimyr): New Geochemical and Isotopic-Geochronological (U-Pb, Sm-Nd) Data. *Dokl. Akad. Nauk. Akad. Nauk* **1998**, *353*, 653–657.
38. Vernikovskiy, V.A.; Sal'nikova, E.; Kotov, A.B.; Ponomarchuk, V.A.; Kovach, V.P.; Travin, A.V.; Yakovleva, S.Z.; Bereznaya, N.G. Age of Post-Collisional Granitoids of Northern Taimyr: U-Pb, Sm-Nd, Rb-Sr, and Ar-Ar Data. *Dokl. Akad. Nauk. Akad. Nauk* **1998**, *363*, 375–378.
39. Proskurnina, M.A.; Proskurnin, V.F.; Remizov, D.N.; Larionov, A.N. Ring Intrusions of the Bepamyatnaya Areal: Manifestations of Shoshonite-Latite Magmatism in Northern Taimyr. *Reg. Geol. Metallog.* **2019**, *76*, 5–22.
40. Khudoley, A.K.; Verzhbitsky, V.E.; Zastrozhnov, D.A.; O'Sullivan, P.; Ershova, V.B.; Proskurnin, V.F.; Tuchkova, M.I.; Rogov, M.A.; Kyser, T.K.; Malyshev, S.V.; et al. Late Paleozoic—Mesozoic Tectonic Evolution of the Eastern Taimyr-Severnaya Zemlya Fold and Thrust Belt and Adjoining Yenisey-Khatanga Depression. *J. Geodyn.* **2018**, *119*, 221–241. [[CrossRef](#)]
41. Lorenz, H.; Gee, D.G.; Whitehouse, M.J. New Geochronological Data on Palaeozoic Igneous Activity and Deformation in the Severnaya Zemlya Archipelago, Russia, and Implications for the Development of the Eurasian Arctic Margin. *Geol. Mag.* **2007**, *144*, 105–125. [[CrossRef](#)]
42. Vernikovskiy, V.A.; Neymark, L.A.; Ponomarchuk, V.A.; Yakovleva, S.Z. New U-Pb, Sn-Nd, Rb-Sr, and K-Ar Ages for the North Taymyr Collisional Granites and Metamorphites. In *Transactions (Doklady) of The Russian Academy of Sciences. Earth Science Sections*; Russian Academy of Sciences: Novosibirsk, Russia, 1996.
43. Makariev, A.A. *State Geological Map of the Russian Federation. Scale 1:1 000 000 (Third Generation)*; Sheet T-45–48th. Cheliuskin; VSEGEI Publishing: St. Petersburg, Russia, 2013.
44. Ershova, V.B.; Anfinson, O.; Prokopiev, A.V.; Khudoley, A.K.; Stockli, D.F.; Faleide, J.I.; Gaina, C.; Malyshev, N.A. Detrital Zircon (U-Th)/He Ages from Paleozoic Strata of the Severnaya Zemlya Archipelago: Deciphering Multiple Episodes of Paleozoic Tectonic Evolution within the Russian High Arctic. *J. Geodyn.* **2018**, *119*, 210–220. [[CrossRef](#)]
45. Morozov, A.F.; Petrov, O. *State Geological Map of the Russian Federation. Scale 1:2500 000*; VSEGEI Publishing House: St. Petersburg, Russia, 2004.
46. Pease, V.L.; Kuzmichev, A.B.; Danukalova, M.K. The New Siberian Islands and Evidence for the Continuation of the Uralides, Arctic Russia. *J. Geol. Soc.* **2014**, *172*, 1–4. [[CrossRef](#)]
47. Harris, N.B.W.; Inger, S.; Ronghua, X. Cretaceous Plutonism in Central Tibet: An Example of Post-Collision Magmatism? *J. Volcanol. Geotherm. Res.* **1990**, *44*, 21–32. [[CrossRef](#)]
48. Wang, Q.; McDermott, F.; Xu, J.F.; Bellon, H.; Zhu, Y.T. Cenozoic K-Rich Adakitic Volcanic Rocks in the Hohxil Area, Northern Tibet: Lower-Crustal Melting in an Intracontinental Setting. *Geology* **2005**, *33*, 465. [[CrossRef](#)]
49. Miller, C.F.; Schuster, R.; Klötzli, U.; Frank, W.; Purtscheller, F. Post-Collisional Potassic and Ultrapotassic Magmatism in SW Tibet: Geochemical and Sr-Nd-Pb-O Isotopic Constraints for Mantle Source Characteristics and Petrogenesis. *J. Pet.* **1999**, *40*, 1399–1424. [[CrossRef](#)]
50. Chung, S.L.; Liu, D.; Ji, J.; Chu, M.F.; Lee, H.Y.; Wen, D.J.; Lo, C.H.; Lee, T.Y.; Qian, Q.; Zhang, Q. Adakites from Continental Collision Zones: Melting of Thickened Lower Crust beneath Southern Tibet. *Geology* **2003**, *31*, 1021. [[CrossRef](#)]
51. Willett, S.D.; Beaumont, C. Subduction of Asian Lithospheric Mantle beneath Tibet Inferred from Models of Continental Collision. *Nature* **1994**, *369*, 642–645. [[CrossRef](#)]
52. Qi, Y.; Wang, Q.; Wei, G.J.; Zhang, X.Z.; Dan, W.; Hao, L.L.; Yang, Y.N. Late Eocene Post-Collisional Magmatic Rocks from the Southern Qiangtang Terrane Record the Melting of Pre-Collisional Enriched Lithospheric Mantle. *Bull. Geol. Soc. Am.* **2021**, *133*, 2612–2624. [[CrossRef](#)]

53. Hadlari, T.; Davis, W.J.; Dewing, K. A Pericratonic Model for the Pearya Terrane as an Extension of the Franklinian Margin of Laurentia, Canadian Arctic. *Bull. Geol. Soc. Am.* **2014**, *126*, 182–200. [[CrossRef](#)]
54. Lorenz, H.; Gee, D.G.; Simonetti, A. Detrital Zircon Ages and Provenance of the Late Neoproterozoic and Palaeozoic Successions on Severnaya Zemlya, Kara Shelf: A Tie to Baltica. *Nor. Geol. Tidsskr.* **2008**, *88*, 235–258.
55. Zonenshain, L.P.; Natapov, L.M. Tectonic History of the Arctic. In *Actual Problems of Continent and Ocean Tectonics*; Nauka: Moscow, Russia, 1987; pp. 31–57.
56. Kuznetsov, N.B.; Natapov, L.M.; Belousova, E.A.; O'Reilly, S.Y.; Griffin, W.L. Geochronological, Geochemical and Isotopic Study of Detrital Zircon Suites from Late Neoproterozoic Clastic Strata along the NE Margin of the East European Craton: Implications for Plate Tectonic Models. *Gondwana Res.* **2010**, *17*, 583–601. [[CrossRef](#)]
57. Metelkin, D.V.; Vernikovskiy, V.A.; Kazansky, A.Y.; Bogolepova, O.K.; Gubanov, A.P. Paleozoic History of the Kara Microcontinent and Its Relation to Siberia and Baltica: Paleomagnetism, Paleogeography and Tectonics. *Tectonophysics* **2005**, *398*, 225–243. [[CrossRef](#)]
58. Vernikovskiy, V.A.; Metelkin, D.V.; Tolmacheva, T.Y.; Malyshev, N.A.; Petrov, O.V.; Sobolev, N.N.; Matushkin, N.Y. Concerning the Issue of Paleotectonic Reconstructions in the Arctic and of the Tectonic Unity of the New Siberian Islands Terrane: New Paleomagnetic and Paleontological Data. *Dokl. Earth Sci.* **2013**, *451*, 791–797. [[CrossRef](#)]
59. Ershova, V.B.; Prokopiev, A.V.; Khudoley, A.K.; Shneider, G.V.; Andersen, T.; Kallerund, K.; Makariev, A.A.; Kolchanov, D.A. U-Pb Dating of Detrital Zircons from the Lower Paleozoic Deposits of the North Kara Basin. *Dokl. Earth Sci.* **2015**, *464*, 444–447. [[CrossRef](#)]
60. Zonenshain, L.P.; Kuz'min, M.I.; Natapov, L.M. *Plate Tectonics of the USSR Territory*; Nedra: Moscow, Russia, 1990.
61. Filatova, N.I.; Khain, V.E. Tectonics of the Eastern Arctic Region. *Geotectonics* **2007**, *41*, 171–194. [[CrossRef](#)]
62. Zonenshain, L.P. *Lithosphere Plates Tectonics within the USSR Territory*; II.; Nedra: Moscow, Russia, 1990.
63. Pogrebitsky, Y.; Lopatin, B.G. *State Geological Maps of the Russian Federation, 1: 1 000 000 New Series (S-47-49). Lake Taimyr*; VSEGEI Publishing: St. Petersburg, Russia, 2000.
64. Ershova, V.B.; Prokopiev, A.V.; Nikishin, V.A.; Khudoley, A.K.; Malyshev, N.A.; Nikishin, A.M. New Data on Upper Carboniferous–Lower Permian Deposits of Bol'shevik Island, Severnaya Zemlya Archipelago. *Polar Res.* **2015**, *34*, 24558. [[CrossRef](#)]
65. Ershova, V.B.; Prokopiev, A.V.; Khudoley, A.K.; Proskurnin, V.F.; Andersen, T.; Kullerud, K.; Stepunina, M.A.; Kolchanov, D.A. New U–Pb Isotopic Data for Detrital Zircons from Metasedimentary Sequences of Northwestern Taimyr. *Dokl. Earth Sci.* **2017**, *474*, 613–616. [[CrossRef](#)]
66. Ershova, V.B.; Prokopiev, A.V.; Khudoley, A.K.; Andersen, T.; Kullerud, K.; Kolchanov, D.A. U–Pb Age and Hf Isotope Geochemistry of Detrital Zircons from Cambrian Sandstones of the Severnaya Zemlya Archipelago and Northern Taimyr (Russian High Arctic). *Minerals* **2020**, *10*, 36. [[CrossRef](#)]
67. Uflyand, A.; Natapov, L.M.; Lopatin, V.; Chernov, D. On the Taimyr Tectonic Nature. *Geotectonics* **1991**, *6*, 76–79.
68. Vernikovskiy, V.A.; Vernikovskaya, A.E.; Pease, V.L.; Gee, D.G. *Neoproterozoic Orogeny along the Margins of Siberia*; Geological Society: London, UK, 2005. [[CrossRef](#)]
69. Priyatkin, N.; Collins, W.J.; Khudoley, A.K.; Zastrozhnov, D.A.; Ershova, V.B.; Chamberlain, K.; Shatsillo, A.; Proskurnin, V.F. The Proterozoic Evolution of Northern Siberian Craton Margin: A Comparison of U–Pb–Hf Signatures from Sedimentary Units of the Taimyr Orogenic Belt and the Siberian Platform. *Int. Geol. Rev.* **2017**, *59*, 1632–1656. [[CrossRef](#)]
70. Sobolevskaya, R.F. New Data on the Stratigraphy of Cambrian Deposits of Central Taimyr. *Proc. NIIGA* **1959**, *101*, 44–49.
71. Khain, V.E.; Sokolov, B.A.; Kleshchev, K.A.; Shein, V.S. Tectonic and Geodynamic Setting of Oil and Gas Basins of the Soviet Union. *Am. Assoc. Pet. Geol. Bull.* **1991**, *75*, 313–325. [[CrossRef](#)]
72. Saunders, A.D.; England, R.W.; Reichow, M.K.; White, R.V. A Mantle Plume Origin for the Siberian Traps: Uplift and Extension in the West Siberian Basin, Russia. *Lithos* **2005**, *79*, 407–424. [[CrossRef](#)]
73. Dobretsov, N.L.; Polyansky, O.P.; Reverdatto, V.V.; Babichev, A.V. Dynamics of the Arctic and Adjacent Petroleum Basins: A Record of Plume and Rifting Activity. *Russ. Geol. Geophys.* **2013**, *54*, 888–902. [[CrossRef](#)]
74. Afanasenkov, A.P.; Nikishin, A.M.; Unger, A.V.; Bordunov, S.I.; Lugovaya, O.V.; Chikishev, A.A.; Yakovishina, E.V. The Tectonics and Stages of the Geological History of the Yenisei–Khatanga Basin and the Conjugate Taimyr Orogen. *Geotectonics* **2016**, *50*, 161–178. [[CrossRef](#)]
75. Krivolutskaya, N.A.; Latyshev, A.V.; Dolgal, A.S.; Gongalsky, B.I.; Makarieva, E.M.; Makariev, A.A.; Svirskaya, N.M.; Bychkova, Y.V.; Yakushev, A.I.; Asavin, A.M. Unique PGE–Cu–Ni Noril'sk Deposits, Siberian Trap Province: Magmatic and Tectonic Factors in Their Origin. *Minerals* **2019**, *9*, 66. [[CrossRef](#)]
76. Williams, I.S. U–Th–Pb Geochronology by ion microprobe. In *Applications of Microanalytical Techniques to Understanding Mineralizing Processes*; Reviews in Economic Geology v.7; Society of Economic Geologists: Littleton, CO, USA, 1998; ISBN 1-887483-51-9.
77. Ludwig, K.R. *SQUID 1.00, A User's Manual*; Berkeley Geochronology Center Special Publication; Berkeley Geochronology Center: Berkeley, CA, USA, 2000; p. 2.
78. Black, L.P.; Kamo, S.L.; Allen, C.M.; Aleinikoff, J.N.; Davis, D.W.; Korsch, R.J.; Foudoulis, C. TEMORA 1: A New Zircon Standard for Phanerozoic U–Pb Geochronology. *Chem. Geol.* **2003**, *200*, 155–170. [[CrossRef](#)]
79. Ludwig, K.R. *User's Manual for Isoplot 3.00, a Geochronological Toolkit for Microsoft Excel*; Berkeley Geochronology Center Special Publication No.4; Berkeley Geochronology Center: Berkeley, CA, USA, 2003.
80. Middlemost, E.A.K. Naming Materials in the Magma/Igneous Rock System. *Earth Sci. Rev.* **1994**, *37*, 215–224. [[CrossRef](#)]

81. Frost, B.R.; Barnes, C.G.; Collins, W.J.; Arculus, R.J.; Ellis, D.J.; Frost, C.D. A Geochemical Classification for Granitic Rocks. *J. Pet.* **2001**, *42*, 2033–2048. [[CrossRef](#)]
82. Whalen, J.B.; Currie, K.L.; Chappell, B.W. A-Type Granites: Geochemical Characteristics, Discrimination and Petrogenesis. *Contrib. Mineral. Petrol.* **1987**, *95*, 407–419. [[CrossRef](#)]
83. Peccerillo, A.; Taylor, S.R. Geochemistry of Eocene Calc-Alkaline Volcanic Rocks from the Kastamonu Area, Northern Turkey. *Contrib. Mineral. Petrol.* **1976**, *58*, 63–81. [[CrossRef](#)]
84. Sun, S.S.; McDonough, W.F. *Chemical and Isotopic Systematics of Oceanic Basalts: Implications for Mantle Composition and Processes*; Geological Society: London, UK, 1989. [[CrossRef](#)]
85. Pearce, J.A.; Harris, N.B.W.; Tindle, A.G. Trace Element Discrimination Diagrams for the Tectonic Interpretation of Granitic Rocks. *J. Petrol.* **1984**, *25*, 956–983. [[CrossRef](#)]
86. Drummond, M.S.; Defant, M.J. A Model for Trondhjemite-Tonalite-Dacite Genesis and Crustal Growth via Slab Melting: Archean to Modern Comparisons. *J. Geophys. Res.* **1990**, *95*, 21503–22152. [[CrossRef](#)]
87. Richards, J.P.; Kerrich, R. Special Paper: Adakite-like Rocks: Their Diverse Origins and Questionable Role in Metallogenesis. *Econ. Geol.* **2007**, *102*, 537–576. [[CrossRef](#)]
88. Berzin, S.V.; Konopelko, D.L.; Petrov, S.V.; Kurapov, M.Y.; Golovina, T.A.; Chernenko, N.Y.; Chervyakovskiy, V.S. Utilizing Compositions of Zircon and Apatite for Prospecting of Cu-Mo-Au-Porphyry Mineralization in the Pekinsky and Tessemysky Granitoid Massifs of the Taimyr-Severozemelskaya Folded Area. *Lithosphere* **2024**.
89. Konopelko, D.; Seltmann, R.; Dolgoplova, A.; Safonova, I.; Glorie, S.; De Grave, J.; Sun, M. Adakite-like Granitoids of Songkultau: A Relic of Juvenile Cambrian Arc in Kyrgyz Tien Shan. *Geosci. Front.* **2021**, *12*, 147–160. [[CrossRef](#)]
90. Hou, Z.Q.; Gao, Y.F.; Qu, X.M.; Rui, Z.Y.; Mo, X.X. Origin of Adakitic Intrusives Generated during Mid-Miocene East-West Extension in Southern Tibet. *Earth Planet. Sci. Lett.* **2004**, *220*, 139–155. [[CrossRef](#)]
91. Rapp, R.P.; Watson, E.B. Dehydration Melting of Metabasalt at 8–32 Kbar: Implications for Continental Growth and Crust-Mantle Recycling. *J. Petrol.* **1995**, *36*, 891–931. [[CrossRef](#)]
92. Qian, Q.; Hermann, J. Partial Melting of Lower Crust at 10–15 Kbar: Constraints on Adakite and TTG Formation. *Contrib. Mineral. Petrol.* **2013**, *165*, 1195–1224. [[CrossRef](#)]
93. Moyen, J.F. High Sr/Y and La/Yb Ratios: The Meaning of the “Adakitic Signature”. *Lithos* **2009**, *112*, 556–574. [[CrossRef](#)]
94. Moyen, J.F. The Composite Archean Grey Gneisses: Petrological Significance, and Evidence for a Non-Unique Tectonic Setting for Archean Crustal Growth. *Lithos* **2011**, *123*, 21–36. [[CrossRef](#)]
95. DePaolo, D.J.; Wasserburg, G.J. Petrogenetic Mixing Models and Nd-Sr Isotopic Patterns. *Geochim. Cosmochim. Acta* **1979**, *43*, 615–627. [[CrossRef](#)]
96. Kovach, V.P.; Kotov, A.B.; Smelov, A.P.; Starosel'tsev, K.V.; Sal'nikova, E.B.; Zagornaya, N.Y.; Safronov, A.F.; Pavlushin, A.D. Evolutionary Stages of the Continental Crust in the Buried Basement of the Eastern Siberian Platform: Sm-Nd Isotopic Data. *Petrology* **2000**, *8*, 353–365.
97. Rosen, O.M.; Levskii, L.K.; Zhuravlev, D.Z.; Rotman, A.Y.; Spetsius, Z.V.; Makeev, A.F.; Zinchuk, N.N.; Manakov, A.V.; Serenko, V.P. Paleoproterozoic Accretion in the Northeast Siberian Craton: Isotopic Dating of the Anabar Collision System. *Stratigr. Geol. Correl.* **2006**, *14*, 581–601. [[CrossRef](#)]
98. Glebovitsky, V.A.; Khil'tova, V.Y.; Kozakov, I.K. Tectonics of the Siberian Craton: Interpretation of Geological, Geophysical, Geochronological, and Isotopic Geochemical Data. *Geotectonics* **2008**, *42*, 8–20. [[CrossRef](#)]
99. Medvedev, A.Y.; Al'Mukhamedov, A.I.; Kirida, N.P. Geochemistry of Permo-Triassic Volcanic Rocks of West Siberia. *Russ. Geol. Geophys.* **2003**, *44*, 86–100.
100. Puchkov, V.N. Structural Stages and Evolution of the Urals. *Mineral. Petrol.* **2013**, *107*, 3–37. [[CrossRef](#)]
101. Biske, G. *Folded Areas of Northern Eurasia. Ural Fold System*; SPbU Publishing: St. Petersburg, Russia, 2004.
102. Konopelko, D.; Klemd, R. Deciphering Protoliths of the (U)HP Rocks in the Makbal Metamorphic Complex, Kyrgyzstan: Geochemistry and SHRIMP Zircon Geochronology. *Eur. J. Mineral.* **2016**, *28*, 1233–1253. [[CrossRef](#)]
103. Biske, Y.S.; Seltmann, R. Paleozoic Tian-Shan as a Transitional Region between the Rheic and Urals-Turkestan Oceans. *Gondwana Res.* **2010**, *17*, 602–613. [[CrossRef](#)]
104. Biske, Y.S.; Konopelko, D.L.; Seltmann, R. Geodynamics of Late Paleozoic Magmatism in the Tien Shan and Its Framework. *Geotectonics* **2013**, *47*, 291–309. [[CrossRef](#)]
105. Konopelko, D.; Biske, Y.S.; Kullerud, K.; Ganiev, I.; Seltmann, R.; Brownscombe, W.; Mirkamalov, R.; Wang, B.; Safonova, I.; Kotler, P.; et al. Early Carboniferous Metamorphism of the Neoproterozoic South Tien Shan-Karakum Basement: New Geochronological Results from Baisun and Kyzylkum, Uzbekistan. *J. Asian Earth Sci.* **2019**, *177*, 275–286. [[CrossRef](#)]
106. Konopelko, D.; Eklund, O. Timing and Geochemistry of Potassic Magmatism in the Eastern Part of the Svecofennian Domain, NW Ladoga Lake Region, Russian Karelia. *Precambrian Res.* **2003**, *120*, 37–53. [[CrossRef](#)]
107. Zhang, X.; Omma, J.; Pease, V.L.; Scott, R.A. Provenance of Late Paleozoic-Mesozoic Sandstones, Taimyr Peninsula, the Arctic. *Geosciences* **2013**, *3*, 502–527. [[CrossRef](#)]
108. Ershova, V.B.; Prokopiev, A.V.; Khudoley, A.K. Devonian–Permian Sedimentary Basins and Paleogeography of the Eastern Russian Arctic: An Overview. *Tectonophysics* **2016**, *691*, 234–255. [[CrossRef](#)]
109. Cocks, L.R.M.; Torsvik, T.H. Siberia, the Wandering Northern Terrane, and Its Changing Geography through the Palaeozoic. *Earth-Sci. Rev.* **2007**, *82*, 29–74. [[CrossRef](#)]

110. Reichow, M.K.; Saunders, A.D.; White, R.V.; Al'Mukhamedov, A.I.; Medvedev, A.Y. Geochemistry and Petrogenesis of Basalts from the West Siberian Basin: An Extension of the Permo-Triassic Siberian Traps, Russia. *Lithos* **2005**, *79*, 425–452. [[CrossRef](#)]
111. Reichow, M.K.; Saunders, A.D.; Scott, R.A.; Millar, I.L.; Barfod, D.; Pringle, M.S.; Rogers, N.W.; Hammond, S. Petrogenesis and Timing of Mafic Magmatism, South Taimyr, Arctic Siberia: A Northerly Continuation of the Siberian Traps? *Lithos* **2016**, *248–251*, 382–401. [[CrossRef](#)]
112. Walderhaug, H.J.; Eide, E.A.; Scott, R.A.; Inger, S.; Golionko, E.G. Palaeomagnetism and  $^{40}\text{Ar}/^{39}\text{Ar}$  Geochronology from the South Taimyr Igneous Complex. Arctic Russia: A Middle-Late Triassic Magmatic Pulse after Siberian Flood-Basalt Volcanism. *Geophys. J. Int.* **2005**, *163*, 501–517. [[CrossRef](#)]
113. Ivanov, A.V.; He, H.; Yan, L.; Ryabov, V.V.; Shevko, A.Y.; Paleskii, S.V.; Nikolaeva, I.V. Siberian Traps Large Igneous Province: Evidence for Two Flood Basalt Pulses around the Permo-Triassic Boundary and in the Middle Triassic, and Contemporaneous Granitic Magmatism. *Earth-Sci. Rev.* **2013**, *122*, 58–76. [[CrossRef](#)]
114. Puchkov, V.N. The Evolution of the Uralian Orogen. *Geol. Soc. Spec. Publ.* **2009**, *327*, 161–195. [[CrossRef](#)]
115. Puchkov, V.N. *Geology of the Urals and Cis-Urals (Actual Problems of Stratigraphy, Tectonics, Geodynamics and Metallogeny)*; Design-Poligraph Service: Ufa, Russia, 2010; ISBN 9785944232090.
116. Kamo, S.L.; Czamanske, G.K.; Amelin, Y.; Fedorenko, V.A.; Davis, D.W.; Trofimov, V.R. Rapid Eruption of Siberian Flood-Volcanic Rocks and Evidence for Coincidence with the Permian-Triassic Boundary and Mass Extinction at 251 Ma. *Earth Planet. Sci. Lett.* **2003**, *214*, 75–91. [[CrossRef](#)]
117. Kuzmichev, A.B.; Pease, V.L. Siberian Trap Magmatism on the New Siberian Islands: Constraints for Arctic Mesozoic Plate Tectonic Reconstructions. *J. Geol. Soc.* **2007**, *164*, 959–968. [[CrossRef](#)]
118. Korago, E.A.; Kovaleva, G.N.; Schekoldin, R.A.; Il'in, V.F.; Gusev, E.A.; Krylov, A.A.; Gorbunov, D.A. Geological Structure of the Novaya Zemlya Archipelago (West Russian Arctic) and Peculiarities of the Tectonics of the Eurasian Arctic. *Geotectonics* **2022**, *56*, 123–156. [[CrossRef](#)]
119. Grahanov, S.A.; Smelov, A.P.; Egorov, K.N.; Suleimanov, A.M.; Nogovicyn, R.R. New Type of Diamond Bedrock Sources in Yakutia. *GeoScience* **2013**, *4*.
120. Grahanov, S.A.; Zinchuk, N.N.; Sobolev, N.V. Age of Projected Bedrock Diamond Sources in the Northeast of the Siberian Platform. *Dokl. Akad. Nauk. Akad. Nauk* **2015**, *465*, 715–719. [[CrossRef](#)]
121. Letnikova, E.F.; Izoch, A.E.; Nikolenko, E.I.; Pochilenko, N.P.; Shelestov, V.O.; Geng, H.; Lobanov, S.S. Late Triassic Stage of Magmatic Activity of High Potassium Trachyte Volcanism in the Northeast of the Siberian Platform: Evidence in Sedimentary Record. *Dokl. Akad. Nauk. Akad. Nauk* **2014**, *459*, 327–331.
122. Ershova, V.; Prokopiev, A.; Andersen, T.; Khudoley, A.; Kullerud, K.; Thomsen, T.B. U–Pb and Hf Isotope Analysis of Detrital Zircons from Devonian–Permian Strata of Kotel'ny Island (New Siberian Islands, Russian Eastern Arctic): Insights into the Middle–Late Paleozoic Evolution of the Arctic. *J. Geodyn.* **2018**, *119*, 199–209. [[CrossRef](#)]
123. Hadlari, T.; Dewing, K.; Matthews, W.A.; Alonso-Torres, D.; Midwinter, D. Early Triassic Development of a Foreland Basin in the Canadian High Arctic: Implications for a Pangean Rim of Fire. *Tectonophysics* **2018**, *736*, 75–84. [[CrossRef](#)]
124. Alonso-Torres, D.; Beauchamp, B.; Guest, B.; Hadlari, T.; Matthews, W. Late Paleozoic to Triassic Arc Magmatism North of the Sverdrup Basin in the Canadian Arctic: Evidence from Detrital Zircon U–Pb Geochronology. *Lithosphere* **2018**, *10*, 426–445. [[CrossRef](#)]

**Disclaimer/Publisher's Note:** The statements, opinions and data contained in all publications are solely those of the individual author(s) and contributor(s) and not of MDPI and/or the editor(s). MDPI and/or the editor(s) disclaim responsibility for any injury to people or property resulting from any ideas, methods, instructions or products referred to in the content.